High-quality assembly of the Chinese white truffle genome and recalibrated divergence time estimate provide insight into the evolutionary dynamics of Tuberaceae

Running title: Tempo and mode of true truffle genome evolution

Jacopo Martelossi[1,2†]*, Jacopo Vujovic[3†], Yue Huang[3,4†], Alessia Tatti[2,5], Kaiwei Xu[4], Federico Puliga[3], Yuanxue Chen[4], Omar Rota Stabelli[2,6,7], Fabrizio Ghiselli[1], Xiaoping Zhang[4‡] & Alessandra Zambonelli[3‡]*

[1]Department of Biological, Geological and Environmental Sciences, University of Bologna, Bologna, 40126, Italy.

[2]Center Agriculture Food Environment (C3A), University of Trento, San Michele all'Adige, Trento, 38010, Italy.

[3]Department of Agricultural and Food Sciences, University of Bologna, Bologna, 40127, Italy

[4]Department of Microbiology, College of Resources, Sichuan Agricultural University, Chengdu, 611130, China.

[5]University School for Advanced Studies IUSS Pavia, Pavia, 27100, Italy.

[6]CIBIO Department, University of Trento, Trento, 38122, Italy.

[7]Research and Innovation Center, Fondazione Edmund Mach, San Michele all'Adige, Trento, 38010, Italy.

[†]Co-First Authors

‡Co-Senior Authors

*Corresponding authors: Jacopo Martelossi - jacopo.martelossi@senckenberg.de; Alessandra Zambonelli - alessandr.zambonelli@unibo.it

Abstract:

The genus *Tuber* (family: Tuberaceae) includes the most economically valuable ectomycorrhizal (ECM), truffle-forming fungi. Previous genomic analyses revealed that massive transposable element (TE) proliferation represents a convergent genomic feature of ECM fungi, including Tuberaceae. Repetitive sequences constitute a principal driver of genome evolution shaping its architecture and regulatory networks. In this context, Tuberaceae can become an important model system to study their genomic impact; however, the family lacks high-quality assemblies. Here, we investigate the interplay between TEs and Tuberaceae genome evolution by producing a highly contiguous assembly for the endangered Chinese white truffle *Tuber panzhihuanense*, along with a recalibrated timeline for Tuberaceae diversification and comprehensive comparative genomic analyses. We find that, concurrently with a Paleogene diversification of the family, pre-existing Chromoviridae-related Gypsy clades independently expanded in different truffle lineages, leading to increased genome size and high gene family turnover rates, but without resulting in highly re-arranged genomes. Additionally, we uncover a significant enrichment of ECM-induced gene families stemming from ancestral duplication events. Finally, we explore the repetitive structure of nuclear ribosomal DNA (rDNA) loci for the first time in the clade. Most of the 45S rDNA paralogues are undergoing concerted evolution, though an isolated divergent locus raises concerns about potential issues for metabarcoding and biodiversity assessments. Our study establishes a fundamental genomic resource for future research on truffle genomics and showcases a clear example of how establishment and self-perpetuating expansion of heterochromatin can drive massive genome size variation due to activity of selfish genetic elements.

Keywords: Long terminal repeats, genome expansion, ribosomal genes, internal transcribed spacer, genome architecture, symbiotic fungi, genomics, ECM, truffle

Introduction

Transposable elements (TEs) and other repetitive sequences are known to be one of the major causes of structural variations within individuals and species, promoting genome expansion, gene duplication, gene loss, genomic rearrangements and reshaping the overall genomic regulatory network (Bourque et al. 2018). Among fungi, true truffles stand out between the most TE-rich species (Muszewska et al. 2019). The family Tuberaceae (Ascomycota: Pezizomycetes) is the richest and most diverse clade of ectomycorrhizal (ECM) truffle-forming fungi (Leonardi et al. 2021) with the genus *Tuber* (true truffles) including some of the most economically valuable species (Leonardi et al. 2021), such as the Périgord black truffle (*Tuber melanosporum* Vittad.) and the Italian white truffle (*Tuber magnatum* Picco) (Mello et al. 2006). Among Tuberaceae, *T. melanosporum* was the first to have its genome sequenced (Martin et al. 2010), revealing one of the larger genomes compared to most of the ascomycetes sequenced at that time. It is characterised by a 4-fold larger genome compared to other ascomycetes and by a high TE content. Comparative genomic analyses of Pezizomycetes (Murat et al. 2018) and various other mycorrhizal-forming fungi (Kohler et al. 2015; Miyauchi et al. 2020) have demonstrated that high TE content and a reduced set of plant cell wall degrading enzymes are recurring genomic features among ectomycorrhizal fungi. As all known Tuberaceae species exhibit an ECM lifestyle (Bonito and Smith 2016), this family represents a valuable model for investigating the genomic impact of transposons and their potential role in shaping phenotypic diversity.

Truffles, typically establish ECM relationships with plants (Tedersoo et al. 2010), are characterised by a hypogeous fruit body where spores are sequestered, and rely on pungent

aromas to attract the animals responsible for their dispersal (Bonito et al. 2013). Most Tuberaceae host plants are angiosperms and presumably these were their ancestral hosts with multiple independent transitions to some gymnosperms (e.g. pines) in individual lineages during their evolution (Bonito et al. 2013). To mitigate TE activity true truffles, rely on a non-exhaustive, partially reversible methylation-based defense, known as the methylation-induced premeiotically (MIP) defence system (Montanini et al. 2014). MIP is more similar to TE control systems of metazoans and plants rather than those of other fungi, such as *Neurospora crassa* Shear & B.O. Dodge which rely on a highly efficient repeat-induced point mutation system (RIP; Galagan and Selker 2004).

High repetitive content imposes great challenges for genome assembly, particularly with short-read technologies, resulting in highly fragmented genomes and unreliable gene and transposon annotations (Peona et al. 2021; Rhie et al. 2021). To date most publicly available Tuberaceae genomes have been produced with short-read data, with the only exception of *Tuber indicum* Cooke & Massee (NCBI accession: GCA_006112555.1) and *Tuber borchii* Vittad. (Murat et al. 2018) which have been sequenced with a combination of PacBio RSII and Illumina short reads. To overcome these limitations and elucidate the impact of transposons bursts in Tuberaceae genomic architecture, we generated a high-quality assembly of the critically endangered Chinese white truffle *Tuber panzhihuanense* X.J. Deng & Y. Wang using PacBio long high-fidelity reads (HiFi). Along with *Tuber latisporum* Juan Chen & P.G, *T. panzhihuanense* is considered one of the most economically important truffle species in China (Wan et al. 2015). Despite its potential economic value, it is currently listed as critically endangered species by the Redlist of China's Biodiversity — Macrofungi (https://english.mee.gov.cn/; Yao et al. 2020; Zhuang et al. 2020). Our assembly represents the most contiguous Tuberaceae genome assembled to date. Leveraging this resource alongside other Pezizomycetes genomes, we a) reconstructed a robust timeline for

Tuberaceae emergence and diversification, b) deciphered the evolutionary dynamics of TEs across the clade, and c) assessed the impact of massive TE bursts on genome architecture and gene family evolution.

Results

A high-quality assembly and gleba-associated microbiome of *Tuber panzhihuanense*

Using *k*-mer based approaches, we estimated a genome size of 109 Mb, compatible with estimates of other *Tuber* species (Murat et al. 2018). As expected for the haploid state of the gleba fruiting body tissue, the genome resulted completely homozygous (Supplemental Fig. S1A). The assembled genome spans 119 Mb with an N50 value of 7.3 Mb, a consensus quality value (QV) of 57.72 and complete single copy BUSCO scores of 96.4%. (Supplemental Table S1; Supplemental Fig. S1B).

Among the 29 assembled contigs, from 1 to 17 encompass almost the entire nuclear genome (Fig. 1A). Contig 18 represents the 302 kb mitochondrial genome, for which we obtained a complete and circularised sequence, while contigs 19–29 contain only 45S rDNA arrays. We found an enrichment of TTAGGG telomere repeats, typical of many eukaryotes including true truffles (Martin et al. 2010), towards both ends of all 17 majors nuclear contigs, except for contigs 16 and 17, which show enrichment only at one end (Supplemental Fig. S2). These two contigs carry 45S rDNA loci at the ends lacking telomeric repeats (see Results section: “45S rDNA genes are organized as a single tandem array with only one diverging locus dispersed throughout the genome”), suggesting that they may represent a single chromosome. These findings indicate that our assembly is close to chromosome-level, with a haploid chromosome number of 1n = 16.

On the 17 nuclear contigs, we predicted 8,701 protein coding genes (PCGs) with a complete and single copy BUSCO score slightly higher than the assembly score (Supplemental Table S1). The *T. panzhihuanense* genome encodes for 363 secreted proteins (SPs) of which 173 are small SP (SSPs) and a reduced set of 198 carbohydrate-active enzymes (CAZys; Supplemental Table S2).

Microbial profiling (Supplemental Fig. S3A) and Blobtools analyses (Supplemental Fig. S3B) for *T. panzhihuanense*, along with other publicly available truffle fruiting bodies, reveal the exclusive presence of ascocarp associated bacteria of the gleba. Bacteria of the genus *Bradyrhizobium* were ubiquitously detected across all species and samples (Supplemental Fig. S3A). Their association with *Tuber* spp. mycelia and fruiting bodies were already described and suggested to be potentially involved in nitrogen fixation (Monaco et al. 2022; Graziosi et al. 2024).

A highly compartmentalised genome dominated by retrotransposons

Manual curation of repeat libraries is considered an important step for accurate transposable elements annotation in non-model species (Goubert et al. 2022; Peona et al. 2024). To improve TE annotation in *T. panzhihuanense* within a reasonable time frame, we manually curated the automatically generated libraries by selecting the most represented consensus sequences and/or those containing detectable protein fragments. Although the curated consensus sequences represent only 18% of the partially curated library, we found that they account for 54% of the total TE content, demonstrating that our selection strategy successfully captured most of the TE complement. While the total TE content did not change much when using the raw versus the partially curated TE library, resulting in both instances over 60%, we observed a drastic reduction in the number of unclassified elements using the former (Supplemental Fig. S4 A,B). Additionally, the curation process yielded significantly

longer consensus sequences compared to the uncurated ones (supplemental Fig. S4C), suggesting a more accurate reconstruction of their complete structure (Peona et al. 2024). Finally, we managed to recover multiple consensus sequences belonging to the Plavaka group of the CMC/CACTA superfamily that were misclassified as LTR/Pao by the automatic annotation of RepeatModeler. Closer inspection of these consensus sequences revealed the presence of 2 bp target site duplications and terminal inverted repeats characterized by the motif 5'-CATAC-3', which are features typical of Plavaka transposons previously identified in other fungal species (Supplemental Fig. S4D; Iyer et al. 2014; Hiltunen et al. 2021).

Regarding the general TE composition, Gypsy long terminal repeats (LTRs) and long interspersed nuclear element (LINE) Tad1, greatly dominate the genomic TE landscape of the Chinese white truffle (Supplemental Fig. S4B). TEs and genes have a strong and significant negative correlation between their densities (Spearman's rho = -0.92; $p < 0.001$; Fig. 1A,B). Moreover, the majority of the assembly is composed of either significantly TE-enriched (TE hotspots; 51% of the genome; mean TE content = 96%) or TE-depleted genomic regions (TE coldspots; 32% of the genome; mean TE content = 15%; Supplemental table S3) with TE hotspots significantly longer than TE coldspots (Welch Two Sample *t*-test, $p < 0.001$; Supplemental Fig. S5). TE hotspots are richer in long retrotransposon insertions, whereas DNA elements are predominant transposons in TE coldspots (Supplemental Fig. S6). Moreover, the latter genomic compartment contains almost all PCGs (7,047), with a gene density of 0.32, 2.6 times higher than the genome wide estimation. These results are mirrored by the distance of TEs from the closest gene (Supplemental Fig. S7A), with DNA transposons more closely associated with genes compared to LINEs and LTRs (Kruskal-Wallis rank sum test, $p < 0.001$; Pairwise Wilcoxon rank-sum test with Bonferroni correction, $p < 0.001$) likely due to the existence of numerous short non-autonomous and/or highly degenerated versions (Supplemental Fig. S7B,C). The classification of almost the entire

genome into these two compartments, along with their striking differences in TE composition, strongly suggests a highly compartmentalized genomic organization. Effector-like small secreted proteins (SSPs) showed no significant enrichment within TE hotspots (sample size = 8701; $X^2 = 1.6749$, $p = 0.25$).

Chromoviridae-related Gypsy elements dominate the repeat landscape in the Chinese white truffle genome

Due to the significant contribution of Gypsy elements to the high TE content in the *T. panzhihuanense* genome, as well as in other true truffles (Payen et al. 2016; Murat et al. 2018), we further investigated their phylogenetic placement and domain structure. Based on network clustering (Supplemental Fig. S8A) and phylogenetic analyses we identified 10 evolutionary distinct families (Fig. 1C; Supplemental Fig. S8B). These families belong to 4 distinct clades: Skipper-Like, TCN-Like, Tmt1, and a rich and diversified clade that we named Prometheus (Fig. 1C; Supplemental Fig. S9). The two former clades correspond to two different elements of the Tmt6 clade founded in Payen et al. (2016), whereas the Prometheus elements correspond to the Tmt3 clade. The Tmt2, Tmt4 and Tmt5 clades identified in Payen et al. (2016) seem to be absent from *T. panzhihuanense*. Similarly to Tmt1 and TCN-Like elements, Prometheus LTRs possess a chromodomain (CHD) and belong to the Chromoviridae Gypsy branch (Supplemental Fig. S10). On the other hand, the identified Skipper-like element, despite its placement with high support in a sister relationship with the reference Skipper transposon (Bootstrap = 88; Supplemental Fig. S9) is lacking the characteristic CHD domain (Supplemental Fig. S10; Marín and Lloréns, 2000). We found that Prometheus is the most abundant Gypsy clade (Fig. 1D) followed by Tmt1, TCN-like, and Skipper-like (Fig. 1D). While most of the Gypsy insertions are composed of degenerated and/or fragmented elements (Supplemental Fig. S11), we also observed 3,066 insertions that almost perfectly match LTR regions of their parent consensus sequence resembling solo-LTR

elements that arise from non-allelic homologous recombination (NAHR) between the two flanking LTRs (Kent et al. 2017).

45S rDNA genes are organized as a single tandem array with only one diverging locus dispersed throughout the genome

The ribosomal-only contigs 19 to 29 (Fig. 2A) display a conserved structural pattern characterized by 45S rDNA genes (18S-5.8S-28S) flanked by a large array of tandemly repeated elements (Fig. 2B,C). We could identify other characteristic motifs: a 160 bp sequence at the 3' end of each rDNA unit with strong similarity to LTR regions of Prometheus Gypsy transposons, whereas at the 5' end before the main tandemly repeated region a 100 bp palindromic structure followed by a smaller GC-rich tandem repeat (Fig. 2C). Beside these 45S rDNA-only contigs, we identified other 4 complete and 2 partial 45S loci with the same structure at one end of contig 16 and contig 17 as well as an additional one isolated along contig 3, 2.8 Mb away from the closest contig end (Fig. 2A). On the other hand, 5S rDNA genes were only identified outside 45S rDNA loci, with a total of 28 copies scattered along multiple contigs (Fig. 2A).

We aligned all 45S rDNA loci and all 5S rDNA genes to evaluate a possible intragenomic variation. 45S rDNA loci identified from contig 16 to contig 29 are highly homogenised, without any insertions or deletions and only 7 positions harbouring variants unique or shared across paralogue copies (Fig. 2D). Instead, the intergenic spacer (IGS) shows variable lengths ranging from 6,312 bp to 8,510 bp mainly due to different copy numbers in the main tandem array (Fig. 2B). Contrary to other 45S loci, rDNA paralogue genes found isolated on contig 3 are more diverging (Fig. 2D). Compared to the 18S_10 and 28S_10 rDNA loci the most diverging regions are the 2 ITS both showing 96% of identity, whereas 18S, 28S, and 5.8 show an identity of 99%, 99%, and 98% respectively. This locus is flanked by 2 IGS regions

238 significantly shorter than those previously described (length of ~3,600 and ~1,600 bp;
239 Supplemental Fig. S12A,B) with one characterized by the insertion of a non-repetitive
240 genomic region of 480 bp of unknown origin, followed by a solo-LTR (Supplemental Fig.
241 S12C,D). On the other hand, 5s rDNA genes present lower sequence similarity levels that can
242 drop down to 80.8% of identity between 5S_14 and 5S_22 paralogues with a mean identity of
243 93.6% (Fig. 2E).

244 **Fossil-calibrated and genome-scale divergence time reveals a late Cretaceous origin and**
245 **Paleogene radiation of Tuberaceae**

246 To provide a robust timeline for Tuberaceae emergence and diversification as well as a
247 backbone for all comparative genomic analyses, we firstly produced a recalibrated divergence
248 time among a set of 32 Ascomycetes, including 8 Tuberaceae (Fig. 3). The species were
249 selected to maximise the number of possible calibration points, allowing us to use the highest
250 number of fossils with clear phylogenetic placement (10 fossil calibrations) to date for an
251 Ascomycota divergence time estimation, assembling a phylogenomic supermatrix of 1,057
252 complete and single-copy BUSCO genes.

253 Generally, we did not observe over- or underestimation of divergence times of Ascomycota
254 and, for most nodes, the use of nucleotide or protein data leads to confidence intervals largely
255 overlapping (Fig. 3), providing evidence on the robustness of our estimates. Such estimates
256 place the origin of the Tuberaceae crown group near the end of the Cretaceous (Mean: ~76
257 million years ago (MYA)), between previous estimations of ~140 MYA (Bonito et al. 2013;
258 Murat et al. 2018) and ~45 MYA (Miyauchi et al. 2020). The dawn of diversification within
259 the genus *Tuber* is instead the Paleogene, around ~56 MYA, which sees the emergence of
260 major subgeneric lineages, the Aestivum clade at ~34 MYA and the Melanosporum clade at

~26 MYA. The estimated split between *T. panzhihuanense* and *T. borchii* (Puberulum clade), its closest relative in the data set, is estimated to have occurred between ~26 and ~30 MYA.

High and variable TE content in Tuberaceae

We estimated the TE content of the 13 included Pezizales species using automatically *de novo* generated libraries. Although we did not manually curate these elements, as previously shown, the overall TE content and its composition did not change significantly when using the raw and partially curated repeat library in the Chinese white truffle genome (Supplemental Fig. S4B), making our results suitable for a genome-wide comparison of the TE content between different species (Carrasco-Valenzuela et al. 2025). Firstly, we explored the presence of possible biases in assembly sizes (as a proxy for genome size) and TE estimations due to different levels of assembly contiguities measured in terms of N50 values, and we did not identify any significant relationship (all $p > 0.05$, Supplemental table S4). Instead, we detected a significant positive correlation between assembly size (proxy for genome size) and both total TE content and Gypsy content, also when correcting for shared evolutionary histories using phylogenetic independent contrasts (Fig. 4A-B, Supplemental table S5; Supplemental table S6). Moreover, for total TE, DNA, and non-Gypsy LTR content, we found strong and significant phylogenetic signals, with Pagel's λ values approaching 1, whereas no such relationship was observed for Gypsy elements (Supplemental Table S6). Indeed, Gypsy LTRs contribute very differently to the overall repeat content, even between closely related *Tuber* species such as *T. melanosporum* and *T. indicum* (Fig. 4C). The four identified clades account for most of the Gypsy content in Tuberaceae, with CHD-related elements being the main contributors (Fig. 4D; Supplemental Table S5), while the relative proportions of the different clades vary greatly among species (Fig. 4D). Lineage-specific

activity of Gypsy clades in *T. panzhihuanense* was confirmed by repeat landscape profiles using a neutral substitution rate of 3.36×10^{-3} per million years (Fig. 4E). We did not produce repeat landscape profiles for other species due to the significantly lower quality of their assemblies; however, an evolutionary scenario mainly involving lineage-specific amplifications was supported by Gypsy phylogenetic analyses with the presence of highly dense species-specific clades that are evolutionarily distant between each other (Fig. 4F).

Members of all 4 Gypsy clades were identified also within Morchellaceae, *Gyromitra esculenta* Pers. ex Fr. and *Pyronema confluens* Tul. & C. Tul. (Supplemental Fig. S13; Supplemental table S5) suggesting their ancestral presence in Pezizomycetes.

Synteny conservation between true truffles and Morchellaceae despite high gene-family turnover rates and TE accumulation

Murat et al. (2018) found a high rate of gene family turnover within Tuberaceae together with an unexpected high level of microsynteny conservation within them. Here, we took advantage of the increased number of truffle genomes together with our high-quality *T. panzhihuanense* assembly to further test these findings and their relationship with TE accumulation. Because no gene annotation was publicly available for *Verpa conica* (O.F. Müll.) Sw. and *G. esculenta* we performed a *de novo* annotation following the same pipeline used for *T. panzhihuanense* (See Supplemental table S7 for summary statistics). Compared to other analysed species, we estimated a 4-fold higher gene family (CAFE λ) turnover rate in Tuberaceae (0.163 vs 0.036; Fig. 5A) with their early evolution mainly impacted by gene losses. However, we also identified 27 significantly expanded gene families in their stem branch (CAFE Viterbi $p < 0.05$; Fig. 5A).

Gene-based synteny analysis between *T. panzhihuanense* and the 16 longest scaffolds of *T. magnatum* confirms a notable conservation of mid-scale synteny within true truffles

(Supplemental Fig. S14A). Moreover, two *T. magnatum* scaffolds align with two different contigs of *T. panzhihuanense*. Considering that all involved contigs possess telomeric repeats at both ends, these rearrangements might reflect chromosomal fusions or fissions. Also, the comparison of *T. panzhihuanense* with the long-read based high-quality *Morchella sextelata* M. Kuo assembly revealed relatively high levels of meso-synteny conservation between the two species (Fig. 5B; Supplemental Fig. S14B). Indeed, 61% of the *T. panzhihuanense* genome and 70% of single copy orthologs resulted syntenic with synteny blocks that can reach up to 2 Mb of length (mean = 269.5 kb; Supplemental Fig. S15A,B). Synteny blocks are markedly elongated in *T. panzhihuanense* relative to *M. sextelata* (Fig. 5E; Wilcoxon rank-sum test, $p < 0.001$) exhibiting up to 20-fold length increases. TE accumulation in intergenic regions emerged as the main driver of synteny block and genome size expansion. While *M. sextelata* shows slightly longer and more numerous introns than *T. panzhihuanense* (Wilcoxon rank-sum test, $p < 0.001$; Supplemental Fig. S16A,B), intergenic regions are on average ~4.8 times longer in *T. panzhihuanense* (Wilcoxon rank-sum test, $p < 0.001$; Supplemental Fig. S14C), with TE accumulation having a much greater impact on their length than on introns (Supplemental Fig. S16D,E). Syntenic genomic regions are slightly but significantly depleted in TEs (TE density: 0.59 vs 0.65; Wilcoxon rank-sum test, $p < 0.01$; (Fig. 5F) and almost two times more gene-dense compared to non-syntenic ones (Gene density: 0.159 vs 0.08; Wilcoxon rank-sum test, $p < 0.01$; Fig. 5G). However, 59% of the TE hotspots are completely contained within synteny blocks and flanked by syntenic genes (Fig. 5C,D). Visual inspection of some of these regions revealed some notable cases of loss of CAZy encoding genes in the *T. panzhihuanense* lineage related to small scale rearrangements (e.g. GH37 and GH39; Fig. 5C) and TE accumulation (e.g. PL1_2; Fig. 5D).

Finally, we found that genes belonging to significantly expanded families in the branch leading to Tuberaceae diversification as well as in *T. panzhihuanense* terminal branch, are

significantly more TE-rich (Wilcoxon rank-sum test, all $p < 0.01$), in their exons, introns, and within 5 kb of flanking sequences (Fig. 5H). Additionally, genes included in TE-hotspots are enriched in paralogous copies of these fast-evolving families (chi-squared test, sample size = 8701, degree of freedom = 1, $X^2 = 149.1907$, $p < 0.01$), with 4.7 times more of these genes than expected by chance. These findings led us to hypothesise that genes located within TE hotspots are likely to be members of multi-copy gene families. Indeed, 54% of the gene content of TE hotspots belongs to families with more than one gene, compared to 18% of the genome.

Gene family expansions at the root of Tuberaceae are related to the establishment of an ectomycorrhizal lifestyle

Gene duplication can lead to neofunctionalization and protein diversification (Copley 2020). We therefore tested whether gene duplication contributed to the transition from a saprotrophic to an ECM lifestyle in the Tuberaceae stem branch. Murat et al. (2018) proposed that conserved ancient gene networks underlie the development and functioning of Tuberaceae ectomycorrhizae. Accordingly, we expect orthologous ECM-induced genes to have retained their function throughout the diversification of the clade. We therefore identified gene families associated with ECM (ECM-induced families) by intersecting our gene family set with genes found to be upregulated in *T. magnatum* ECM compared to free-living mycelium by Murat et al. (2018). In total, we identified 328 gene families containing *T. magnatum* ECM-induced orthologues, of which 18 are expanded, and 5 of these are significantly expanded in the branch of interest (Fig. 6A; Supplemental Table S8; Supplemental Fig. S15). We then applied a Fisher's exact test to assess the hypothesis that ECM-induced gene families are significantly overrepresented among expanded and significantly expanded gene families in the stem branch of Tuberaceae. Contingency tables were constructed by counting the number of ECM-induced and non-ECM-induced gene

359 families in the expanded/significantly expanded categories versus all other gene families
360 having at least one gene in one Tuberaceae species (i.e present at the root of Tuberaceae). In
361 both instances we found a significant overrepresentation of ECM-induced gene families of
362 2.5-fold and 3.7-fold among respectively expanded ($p < 0.001$) and significantly expanded
363 gene families ($p = 0.013$).

364 Significantly expanded gene families of particular interest are the OG0000007, OG0000028,
365 and OG0000075 (Fig. 6A,B). The former encodes for NOD-like receptors (NLRs) and a total
366 of 187 genes are clustered in this family, with only 1 orthologue in *P. confluens* and 1 in *V.*
367 *conica.* Morchellaceae have apparently lost this gene family, whereas Tuberaceae possess a
368 variable but high number of paralogous copies. The other two gene families encode for
369 putative Ras-like and But2 C-terminal-like proteins, respectively. For the former family,
370 Tuberaceae species encodes between 6 and 30 genes whereas other Pezyzomicetes between 3
371 and 0. For the latter family, Tuberaceae species encode at least 5 gene copies, except for *T.*
372 *panzhihuanense*, which appears to have lost this gene family. In other analysed species, there
373 are between 1 and 3 copies. All Tuberaceae But2 C-terminal-like genes encode for SSP. The
374 two remaining significantly expanded ECM-induced gene families OG0000009 and
375 OG0000138 encode, respectively, ankyrin repeat–containing proteins and AAA ATPases
376 (Supplemental Fig. S17).

377 ## Discussion

378 This study presents a high-quality genome assembly for the critically endangered Chinese
379 white truffle, *Tuber panzhihuanense*, exhibiting a contiguity approximately fourfold higher
380 than that of the second most contiguous *Tuber* genome (*T. magnatum* GCA_003182015.1,
381 scaffold N50 of 1.8 Mb and contig N50 of 45.1 kb). Its high assembly quality, our
382 recalibrated divergence time, and in-depth analyses of TEs and gene family evolution across

Pezizales, allowed us to explore with unprecedented detail the impact of massive TE burst in genome architecture and evolution of Tuberaceae.

Based on multiple fossil calibration points and a genome-scale matrix, we placed the diversification of Tuberaceae and true truffles in a more biologically meaningful timeframe compared to previous studies (Bonito et al. 2013; Murat et al. 2018: Miyauchi et al. 2020) which were based on substitution rates inferred from distantly related taxa and/or few fossil data. A late Cretaceous emergence of the family is consistent with the angiosperm terrestrial revolution (Benton et al. 2022) that gave rise to the most species-rich living clades of angiosperms (Ramírez-Barahona et al. 2020), mammals (Álvarez-Carretero et al. 2022), birds (Jarvis et al. 2014) and arthropods (Benton et al. 2022; Montagna et al. 2019) but their following diversification took place in the Paleogene. The diversification of truffles therefore occurred in a context of expanding angiosperm-based ecosystems in which these fungi coevolved and codiversified with their host plants and the animals responsible for their spore dispersal (Benton et al. 2022; Brundrett and Tedersoo 2018). It is noteworthy that within Basidiomycota, ECM Agaricomycetes apparently experienced a similar evolutionary course, diversifying rapidly during the Paleogene following a late Cretaceous divergence (Sato 2024).

Massive TE bursts, triggered by horizontal transposon transfer or stochastic activation of pre-existing lineages, can lead to rapid genome size increases (Schaack et al. 2010; Oggenfuss et al. 2021). Previous studies have already highlighted the prominent role of Gypsy elements—particularly chromoviridae-related clades—in driving genome expansion in true truffles (Martin et al. 2010; Payen et al. 2016; Murat et al. 2018; Miyauchi et al. 2020). However, whether these bursts represent ancestral or lineage-specific events, and which specific clades were involved, has remained an open question. Here, we found that Tuberaceae genomes host

four main CHD-related clades which underwent predominantly lineage-specific activity. Together with the presence of representative elements in several other Pezizales species, this makes Tuberaceae an iconic example of how an apparently common genome size expansion within a clade can be driven by parallel genomic trajectories, involving the differential lineage-specific proliferation of pre-existing transposon lineages—possibly influenced by specific demographic dynamics (Murat et al. 2010).

Reduced gene density is a widely observed result of TE accumulation (Muszewska et al. 2019). Our results indicate that, in Tuberaceae, this is due to a highly compartmentalized genome architecture, with stretches of heterochromatic DNA dominated by long retrotransposon insertions interspersed with compact, gene-rich regions. The absence of an enrichment of SSPs within TE-rich regions suggest a partially different genomic organization compared to the frequent TE/effector compartmentalisation of pathogenic fungi genomes (Raffaele et al. 2010; Schmidt et al. 2013; Fouché et al. 2020). Non-random distribution of TEs, particularly Gypsy LTRs, was already observed in *T. melanosporum* (Martin et al. 2010; Payen et al. 2016) and chromoviridae-related LTRs are known to have a strong preference for heterochromatic genomic regions in plants (Neumann et al. 2011) and in the fungus *Schizosaccharomyces pombe* Lindner, where the CHD domain directly recognizes histone H3 K9 methylation (Gao et al. 2008). Increased genome size of Tuberaceae is therefore the result of a process of retrotransposons-mediated self-perpetuating expansion of heterochromatic genomic regions (Gao et al. 2008), rather than intron gain or intron expansion, as observed in other eukaryotes (Cicconardi et al. 2023). No heterochromatic insertion preference has been described so far for LINE Tad1 elements, and their massive presence within these regions can be explained by negative selection against long insertions in gene-dense genomic regions (Buckley et al. 2017; Ruggieri et al. 2022; Martelossi et al. 2024). Similarly to what was previously observed in the fungus *Pleurotus ostreatus* (Jacq.) P. Kumm. (Castanera et al.

2016), we found evidence of NAHR between LTR regions of Gypsy transposons. We therefore suggest that Tuberaceae genomes coped with TE expansions both due to strong insertion preference of highly active Gypsy elements and, on the host genome side, due to MIP and an increased rate of ectopic recombination resulting from the spread of homologous sequences throughout the genome, limiting the deleterious effects of an uncontrolled proliferation.

The emergence of non-homologous and rearranged genomic regions can be another major outcome of TE bursts (Thon et al. 2006; Aguileta et al. 2009; Treindl et al. 2021). However, the massive, lineage-specific activity of Chromoviridae-related Gypsy elements during Tuberaceae diversification did not result in extensive genome re-arrangements, as indicated by the strong conservation of synteny between *T. panzhihuanense* and *T. magnatum*, and even between *T. panzhihuanense* and *M. sextelata*—a Morchellaceae species that diverged from Tuberaceae ancestor over 200 million years ago and characterized by low TE content and high gene density (Han et al. 2019). Instead, rampant TE accumulation primarily elongates syntenic blocks while preserving mid-scale synteny, with the occasional emergence of small-scale genomic rearrangements, possibly favouring the establishment of novel TE-rich heterochromatic DNA. Indeed, multiple CAZy enzymes encoded by *M. sextelata* were lost and replaced by TE-rich genomic regions in *T. panzhihuanense*, suggesting that TE insertions, together with sequence decay (Murat et al. 2018), might have contributed to gene loss in the clade. Despite the absence of chromosome-scale assemblies to dissect intra- and inter-chromosomal genomic rearrangements, our results recapitulate the mesosynteny pattern formally described in filamentous fungi (Hane et al. 2011) and observed between *T. melanosporum* and the Eurotiomycete *Coccidioides immitis* Rixford & Gilchrist (Martin et al. 2010). Furthermore, the presence of 16 putative chromosomes in the haploid genome of *T. panzhihuanense*, along with its syntenic relationships with *T. magnatum*, suggests that, while

457 mesosynteny is maintained, large-scale chromosomal rearrangements—such as fusions and
458 fissions—might have occurred during Tuberaceae diversification. To date, cytogenetic data
459 are available for only four *Tuber* species with an estimated haploid chromosome number
460 ranging from 4 to 5 (Poma et al. 1998; Poma et al. 2002). Additional cytogenetic and/or
461 chromosome conformation capture data on *T. panzhihuanense* and other true truffles will be
462 necessary to confirm our findings and assess the impact of large-scale genomic
463 rearrangements on Tuberaceae genome evolution.

464 The preferential localization of multi-copy gene families within TE-rich genomic regions
465 supports the idea that these regions act as hotspots for copy number variation (Montanini et
466 al. 2014). The overrepresentation of ECM-induced gene families among those significantly
467 expanded on the stem branch of the family further suggests that protein diversification
468 through neo- and/or subfunctionalization may have contributed to the emergence of the ECM
469 lifestyle. Based on the annotated domains, these gene families appear to be involved in
470 self/non-self-recognition, signal transduction, and the modulation of transcription in both the
471 fungus and eventually its host. Indeed, rapid adaptation to a changing environment during
472 ECM establishment has been suggested to involve signal transduction pathway cascades
473 (Martin and Tunlid 2009), potentially including NLRs, Ras-like proteins, and But2 C-
474 terminal-like proteins. NLRs are a class of receptor proteins involved in various types of
475 biotic interactions, including self/non-self-recognition and ECM symbiosis (Dyrka et al.
476 2014), and many NLR-encoding genes were found upregulated in *T. melanosporum* during
477 ECM formation (Martin et al. 2010). The genome of the ECM fungus *Laccaria bicolor*
478 (Maire) P.D.Orton encodes a wide set of protein kinase and RAS small guanosine
479 triphosphatase (GTPase) genes (Martin et al. 2008), with frequent neofunctionalization of
480 paralogous copies and few pseudogenization events (Rajashekar et al. 2009). The expression
481 of one of these genes, *Lbras*, depends on the interaction with host roots and it is expressed in

established mycorrhizal tissues (Sundaram et al. 2001). But proteins of *Saccharomyces cerevisiae* Meyen ex E.C. Hansen are seemingly involved in the activation of the NEDD8 ligation pathway, which leads to substrate NEDDylation (Yashiroda and Tanaka 2003), a post-translational modification that is crucial for fungal cellular processes such as development and secondary metabolism (Yang et al. 2022). SSP proteins with high similarity to But2 C-terminal domain could be involved, with other fungal secreted proteins, in affecting host transcription and responses needed for the establishment and retention of mycorrhizal structures or part of fungal-host plant crosstalk.

Finally, we explored the structure of nuclear rDNA loci, which were difficult to characterise in previous genome assemblies due to their low contiguity. The high level of similarity found between 45S rDNA genes and the presence of partial arrays only at the ends or within rDNA-only contigs, suggest that the 45S genes are undergoing concerted evolution due to high homogenization within a single cluster (Ganley and Kobayashi 2011; Hori et al. 2021; Garcia et al. 2024). The complex IGS region, similarly to what is observed in humans and budding yeast (Ganley and Kobayashi 2011; Hori et al. 2021), is composed of tandemly arranged repeats and can undergo deletion and duplication events, leading to rDNA arrays of different lengths. IGS regions contain regulatory sequences involved in rDNA maintenance, replication and transcription (Hori et al. 2024). The variability of the spacers has also been correlated with differential expression of rDNA loci (Kim et al. 2024) due to its potential impact on functional elements that are embedded in the structure of the sequence. We also provide evidence of intragenomic variability of 45S rDNA units, with the identification of one diverging copy that is located outside the presumptive main cluster. As observed in Robicheau et al. (2017), the isolated rDNA copy might have emerged through nonhomologous exchange of centromeric sequences in proximity to rDNA arrays or eventually by a recombination event fostered by the tandemly repeated sequences of the IGS,

with the subsequent accumulation of point mutations due to weaker concerted evolution. Its existence should not invalidate the use of the ITS region for species and strain identification in *T. panzhihuanense* using classic Sanger sequencing, as, even if we assume a successful primer binding, most of the fluorescent intensity of the electropherogram would come from the paralogous copies of the main clusters. However, it can become a problem with metagenomics studies based on environmental DNA samples (Bradshaw et al. 2023). We therefore encourage future investigation of the 45S rDNA gene polymorphisms in truffles to avoid the establishment of new cryptic species and invalid diversity estimates due to intra-genomic polymorphisms.

The high-quality *T. panzhihuanense* assembly will represent a fundamental resource for future agriculture-applied studies of this endangered species (e.g., transitioning this currently uncultivable species from wild harvesting to orchard cultivation, Lemmond et al. 2023) and will continue to serve as a basis for genomic studies of truffles.

Materials and Methods

Sampling and DNA/RNA sequencing

The sample used for genome sequencing was collected in 2020 by the Jinsha river basin (river section of Zhongba village, Renhe district, city of Panzhihua, China). The fruiting body was isolated and taxonomically identified based on morphology and molecular characteristics and sent to Personalbio Co., Ltd. (Shanghai, China) for whole Genome Sequencing (WGS). WGS was performed both on a PacBio Sequel II obtaining 38+ Gb of HiFi reads and on an Illumina NovaSeq 6000 platform. RNA-seq data used for genome annotation were obtained from 3 replicates of each 100 individual ECMs isolated from one *P. massoniana-T. panzhihuanense* mycorrhizal seedlings. Samples were sent to Novogene Technology Co.,

Ltd. (Beijing, China) for library construction and sequencing on an Illumina NovaSeq 6000 platform in 150 PE mode. For detailed sample identification, mycorrhizal synthesis preparation and library construction, see the Supplemental Methods.

Genome survey and assembly

Illumina reads were quality checked with FastQC v0.11.7 (Andrews 2010) and trimmed with Trimmomatic v0.39 (Bolger et al. 2014) (*-phred33 LEADING:3 TRAILING:3 SLIDINGWINDOW:4:15 MINLEN:36*). Trimmed reads were used with KAT v2.4.2 (Mapleson et al. 2017) *hist* to produce *k*-mer frequency histogram. Genome size and heterozygosity were estimated with GenomeScope 2.0 (Ranallo-Benavidez et al. 2020). PacBio subreads were processed to obtain final CCS (Circular Consensus Sequences) reads using PacBio CCS tool v6.4.0 (*--min-rq 0.99*). The genome was assembled with Hifiasm v0.16.1 (Cheng et al. 2021) under default parameters, and Blobtools v1.1 (Laetsch and Blaxter 2017) was used to identify contigs deriving from fruiting body-associated microorganisms. To obtain coverage information, we mapped HiFi reads back to the assembly with minimap2 v2.24-r1122 (Li 2018) (*-ax map-hifi*), while for taxonomic annotation, we blasted all contigs against the NCBI nt database (*BLASTN -max_target_seqs 10 -max_hsps 1 -evalue* 1×10^{-25}). Reads mapped to identified microorganisms-associated contigs were excluded, and the genome was reassembled with Hifiasm. TTAGGG telomeric repeats were identified with tidk (Brown et al. 2025) under default settings. Quality and completeness of the final assembly were assessed with BUSCO v5.2.2 (Mosè et al. 2021; fungi_odb10 reference database) and Merqury (Rhie et al. 2020) with a *k*-mer size of 21. Metagenomic taxonomic profiling was performed using raw short reads from our study, along with publicly available sequencing data from the gleba of *T. brumale*, *T. indicum*, and *T. melanosporum*. A *T. borchii* isolate was used as a control. Paired-end sequencing reads

were classified using Kraken2 v2.1.2 (Wood et al. 2019) with a custom Kraken database built from merged bacterial and fungal genomes downloaded from NCBI RefSeq. For details about Kraken2 classification see Supplemental Methods.

Repeat annotation

For repeat annotation, we produced a starting raw repeat library with RepeatModeler2 v2.0.4 (Flynn et al. 2020) with the LTR structure extension. Raw consensus sequences were used for a first genome annotation with RepeatMasker v4.1.2-p1 (Smit 2013-2015) in sensitive mode (*-s*). Based on RepeatMasker results, we isolated all consensus sequences with at least 50 instances in the genome and/or characterised by protein fragments based on Blastx (E-value 1×10^{-5}) results against the RepeatPeps database from the RepeatMasker package. Selected sequences were subjected to manual curation and classification based on structural features (presence and length of target site duplications, presence of terminal inverted repeats or long terminal repeats, and TE-related domains identified through the NCBI Conserved Domain Database) following a "Blast-Extend-Extract" process as described in Goubert et al. (2022) and Peona et al. (2024). Curated and uncurated consensus were merged and redundancy removed following the 80-80 rule (i.e. requiring a minimum 80% identity along 80% of the shortest sequence; Wicker et al. 2007; Goubert et al. 2022) with cd-hit-est (*-c 0.8 -n 5 -aS 0.8 -g 1 -G 0 -t 1*). This partially curated library was used for repeat annotation and soft masking the genome with RepeatMasker in sensitive mode. We post-processed RepeatMasker results with the parseRM.pl script (https://github.com/4ureliek/Parsing-RepeatMasker-Outputs/blob/master/parseRM.pl) to obtain genome-wide repeat estimations and RepeatCraft (Wong and Simakov 2019) in *loose* mode to defragment closely spaced repeat loci and obtain a final TE annotation.

Gene annotation

Quality of RNA-seq reads was assessed with FastQC v0.11.7 and trimmed with Trimmomatic v0.39 (-phred33 LEADING:3 TRAILING:3 SLIDINGWINDOW:4:15 MINLEN:36). We assembled the transcriptome with Trinity v2.1.1 (Grabherr et al. 2011) under default parameters.

For gene annotation, we used Funannotate v1.8.16 (Palmer and Stajich 2019) on the soft-masked version of the genome performing an *ab-initio* gene prediction with AUGUSTUS (Stanke et al. 2008), SNAP (Korf 2004), GlimmerHMM (Majoros et al. 2004), CodingQuarry (Testa et al. 2015) and GeneMark-ES (Lomsadze et al. 2005). As external evidences, together with the assembled transcriptome, we selected a high-quality and consistent set of proteins composed by 4 Ascomycota RefSeq proteomes available on NCBI (GCF_000151645.1: *Tuber melanosporum*, GCF_003444635.1: *Morchella importuna*, GCF_020137385.1: *Morchella sextelata*, and GCF_024521635.1: *Tricharina praecox*) and the Swiss-Prot database (The UniProt Consortium 2023). We excluded other available *Tuber* spp. gene annotation available on NCBI as the gene annotation is not part of the RefSeq collection (https://www.ncbi.nlm.nih.gov/refseq/annotation_euk/process/).

Functional annotation of predicted genes was performed with InterProScan V5.70 (Jones et al. 2014) to obtain Pfam domains (Mistry et al. 2021) and InterPro entries. CAZymes were separately annotated with dbCAN3 (Zheng et al. 2023). rDNA genes were annotated using RNAmmer (Lagesen et al. 2007). SPs were annotated following the method of Pellegrin et al. (2015). We considered SP proteins as SSPs when their length was equal to or lower than 300 aa, as in Pellegrin et al. (2015).

TE genomic distribution analyses

To test the interplay between gene density and TE densities we subdivided the *T. panzhihuanense* nuclear genome into non-overlapping windows of 50 kb using BEDTools *makewindows* (Quinlan and Hall 2010) and calculated the proportion of base pairs occupied by genes and transposons for each interval.

To detect genomic regions significantly enriched (TE hotspots) and depleted (TE coldspots) in TEs we applied a binomial test on the number of base pairs occupied by transposons in genomic sliding windows of 20 kb with a window step size of 5 kb. For each window, we computed the TE coverage using BEDTools *coverage* and compared the observed number with the genome-wide average estimation computed across all windows. For each genomic interval, we separately tested for both significant greater and lower TE content compared to genome-wide estimation as alternative hypotheses, generating two sets of intervals representing genomic regions significantly enriched and depleted in TEs, respectively. *P*-values were corrected for multiple testing with the Benjamini–Hochberg procedure and a false discovery rate (FDR) cut-off of 0.01. Because applying a sliding window approach may result in overlapping genomic intervals being annotated as both TE-rich (TE hotspots) and TE-depleted (TE coldspots), we used BEDTools *subtract* reciprocally on both interval sets to remove overlapping regions. Genes completely falling within TE-enriched or TE-depleted windows were extracted using BEDTools *intersect* (-f 1).

Identification, classification, and annotation of LTR Gypsy families

We reconstructed *T. panzhihuanense* Gypsy families from the evolutionary relationships of RT domains of single insertions. RT nucleotide segments >400 nt and the corresponding protein sequences were retrieved via BLASTx (E-value ≤ 1×10□ □) of all LTR insertions

against RT domains from GypsyDB (Llorens et al. 2011) and confirmed via BLASTP (E-value ≤ 1×10□ □) against the RepeatPep library, retaining only best hits to Gypsy elements.

For phylogenetics, confirmed RT protein sequences were clustered with CD-HIT (-c 0.8), aligned with MAFFT v7.520 (G-INS-i), and trimmed with trimAl (-gt 0.8). A maximum likelihood tree was inferred with IQ-TREE v2.2.2.6, using ModelFinder for model selection and 1,000 ultrafast bootstrap replicates (Hoang et al. 2018) for assessing nodal support.

To complement the phylogenetic analyses, we built a network from all-to-all BLASTN (E-value ≤ 1×10□ □) of RT nucleotide sequences; alignments <300 bp were excluded. Bit scores were used as edge weights to detect communities with greedy_modularity_communities function of the NetworkX Python package (Hagberg et al. 2008). Gypsy communities were mapped onto the RT phylogeny, and families defined as well-supported (Bootstrap ≥75) divergent clades, splitting communities where necessary.

To build consensus sequences representative of the identified families, we recovered all insertions from which the RT segments used in the phylogenetic analyses were derived and aligned them separately with MAFFT v7.520. From these alignments, we generated initial consensus sequences with CIAlign (Tumescheit et al. 2022), refined them using a 'Blast-Extend-Extract' process as previously described, and finally assessed their completeness with TE-aid (Goubert et al. 2022).

We classified curated Gypsy families relying on phylogenetic relationships with previously described elements. RT protein domains extracted from each consensus were added to a set of reference Gypsy elements including known Gypsy clades described in GypsyDB and elements from Novikova et al. (2010), Riccioni et al. (2008) and Payen et al. (2016). To identify representative elements of the six Gypsy lineages described by Payen et al. (2016), we isolated the RT segments from all Gypsy sequences mined by the authors based on

BLASTX alignment coordinates, as previously described. All mined Gypsy sequences were then clustered at 80% identity at the protein level using CD-HIT. All sequences were aligned with MAFFT G-INS-i and gappy positions removed with trimAl (*-gt* 0.8). We inferred a ML tree with IQ-TREE together with ModelFinder and 1,000 UltraFastBootstrap replicates. Each Gypsy family was assigned to the closest known clade if the bootstrap value was ≥ 75.

Classified Gypsy families were used in an additional RepeatMasker analysis in sensitive mode and results were post-processed to obtain their genome-wide estimations and repeat landscapes, as previously described. We used the parseRM.pl script to produce a repeat landscape describing the activity of transposons through absolute time using a Tuber-specific neutral substitution rate (See Material and Methods: Phylogenomics and divergence time estimation).

To identify solo-LTRs arising from NAHR events, we blasted back (BLASTN, E-value 1×10^{-5}) all insertions against their source consensus sequence and identified alignments that reciprocally cover both the insertion and one of the two LTR regions of the source consensus for at least 90% of their length. If the alignment reciprocally covers the insertion and the whole consensus sequence for 90% of their length, we considered the elements as full-length, and all other instances were considered as degenerated and/or fragmented elements.

Comparative genomics analyses

Phylogenomics and divergence time estimation

We performed species tree inference across a dataset of 31 Ascomycetes genomes available on NCBI. Species were chosen to have as many calibration points as possible for the divergence time estimation (Supplemental table S9).

We extracted single-copy orthologous genes from all 31 fungal genomes using BUSCO and the Ascomycota_odb10 reference database. Amino acid and nucleotide sequences of complete and single-copy BUSCO genes present in at least 95% of the species were aligned using MAFFT in auto mode and cleaned of gappy positions with trimAl (-automated1). Single-gene amino acid alignments were then concatenated and subjected to maximum likelihood (ML) tree inference with IQ-TREE, incorporating ModelFinder2 and 1,000 UltraFast Bootstrap replicates.

To obtain a reliable timeframe for Ascomycota and, specifically, truffle diversification, we applied a Bayesian approach using multiple fossil calibrations as priors on our genome-scale dataset and the previously inferred species tree, as implemented in the MCMCTree package (dos Reis and Yang 2019). Specifically, we used 10 fossils with unambiguous phylogenetic placements, fitting a flat distribution between minimum and maximum bounds, and a normal distribution for the root of the tree (split between Taphrinomycotina and Saccharomycotina + Pezizomycotina). All priors are detailed in Supplemental Table S10, along with a deep justification for each fossil in Supplemental Methods. Three runs were performed under an independent rates model, and convergence of the MCMC chains was assessed using Tracer (Rambaut et al. 2018). MCMCTree was run on both amino acid and nucleotide alignments to assess the sensitivity of the analyses to the underlying dataset.

To estimate a putative neutral substitution rate for Tuberaceae, we extracted all 4-fold degenerate sites from the previously identified Tuberaceae BUSCO genes and concatenated them. LSD2 (To et al. 2016) within IQ-TREE2 was then used to estimate a fixed substitution rate within the Tuberaceae subtree, calibrating all nodes setting as maximum and minimum bound the 95% highest posterior density estimation obtained from MCMCTree analyses on the nucleotide alignment.

Repeat annotation and analyses across additional Pezizales genomes

All Pezizales genomes included in phylogenetic analyses were used in a *de novo* repeat discovery with RepeatModeler2 and the LTR structure extension. Raw species-specific repeat libraries were used for repeat annotation in each genome with RepeatMasker in sensitive mode to obtain a rough estimation of their repetitive content. Relationships between genome size, and TE content were assessed with correlation analyses to the raw and to the data corrected for shared evolutionary histories using phylogenetic independent contrasts (PIC) with the *pic* function of Ape R (R core team 2021) package (Paradis et al. 2004). Phylogenetic signal was tested with Pagel's λ (Pagel 1999) with the *phylosig* function of the Phytools R package (Revell 2024).

To characterise the distribution of different Gypsy clades across Pezizales diversity, we classified all Gypsy consensus sequences following the same approach used to classify Gypsy families isolated from the *T. panzhihuanense* genome after adding the *T. panzhihuanense* classified Gypsy families to the reference RT database.

Classified consensus sequences mined from Tuberaceae species were subjected to manual curation following a "Blast-Extend-Extract" process, as previously described. Curated consensus was used in an additional RepeatMasker analysis on their source genome to obtain an accurate estimation of their genomic occurrence. RT fragments longer than 400 nt were extracted from the annotation (BLASTX; E-value 1×10^{-5}) and elements coming from Prometheus, Tmt1 and TCN-like clades were separately aligned via MAFFT in G-INS-i mode and, after removing gappy positions with trimAl (*-gt* 0.8), subjected to phylogenetic inference with FastTree v2.1.10 (Price et al. 2010) under a GTR + Gamma model.

Gene family evolutionary analyses and syntenic genomic region detection

Syntenic genomic regions between *T. panzhihuanense* and the 16 longest scaffolds of *T. magnatum* (GCA_003182015.1) and between *T. panzhihuanense* and *M. sextelata (*GCF_024521635.1*)* genomes were identified with GENESPACE v1.3.1 under default parameters (Lovell et al. 2022) after excluding the identified rDNA contigs of *T. panzhihuanense*. A riparian plot was generated from inferred syntenic blocks with the *plot_riparian* function, with the length of the block proportional to its actual length in base pairs. Syntenic and non-syntenic orthologs were extracted from GENESPACE results with the *query_pangenes* function.

We studied gene family turnover dynamics during Pezizales diversification using CAFE5 (Mendes et al. 2020) and the corresponding nucleotide divergence time estimation as a background tree. Gene family counts were obtained by inferring orthogroups from the proteomes of all species with OrthoFinder v2.5.5 (Emms and Kelly 2019) with diamond (Buchfink et al. 2015) in ultra-sensitive mode (*-S diamcond_ultra_sens*). Because no gene annotation was freely available for *Verpa conica* (GCA_033030425.1) and *Gyromitra esculenta* (GCA_038503075.1), we performed a *de novo* annotation using Funannotate following the previously described procedure for *T. panzhihuanense*. Briefly, RNA-seq reads were downloaded from NCBI (SRR12605086 and SRR5491178 for *V. conica* and *G. esculenta*, respectively) and the transcriptomes were assembled with Trinity v2.1.1 (default mode). Assembled transcripts and previously described protein evidence (See Material and Methods: “Gene annotation”) were then supplied to Funannotate as external evidence. Gene family turnover analyses were performed, estimating an error model and specifying two separate lambdas (λ) for the tree, one for Tuberaceae and one for other Pezizales branches.

Spatial relationships between TEs, syntenic genomic regions, and fast-evolving gene families

To explore the spatial relationships between TEs, synteny, and gene family evolution, we looked at the genomic occurrence of transposons based on the RepeatMasker analyses obtained with the curated TE library on the *T. panzhihuanense* genome. After extracting syntenic and non-syntenic genomic regions between *T. panzhihuanense and M. sextelata* from GENESPACE results, we compared their gene and TE density across non-overlapping genomic windows of 50 kb. Accumulation of TEs in significantly expanded/contracted gene families was tested by looking at the percentage of base pairs annotated as TEs across exons, introns and 5 kb flanking regions compared to the rest of the genes.

Data Access

The sequencing data generated in this study have been submitted to the NCBI BioProject database (https://www.ncbi.nlm.nih.gov/bioproject/) under accession number PRJNA1110184. The *T. panzhihuanense* genome assembly, all gene annotations, as well the transposable element libraries and orthogroup clusters described in this article are available on Figshare at https://figshare.com/s/a435a5ac8371bcea2cae and as Supplemental Data.

Competing interest statement

The authors declare no competing interests.

Acknowledgments

The authors would like to thank China Scholarship Council-University of Bologna Cooperation Scholarship. Part of the research was completed thanks to the Master of Science course in Microbiology, China, with the relevant degree thesis [Biological Traits of

Occurrence of Chinese Truffles (*Tuber* spp.) in the Natural Truffle Producing Area of Jinsha River Basin, China] confidential until June 2025 at https://www.cnki.net/index/.

Fundings

The topic was selected as one of the 2016-2017 Sichuan Agricultural University Subject Construction Dual Support Projects (Special funding projects for outstanding young researchers) led by Y.H. and X.Z. This work was partially supported by the "Canziani Bequest" fund, University of Bologna (grant number A.31.CANZELSEW) funded to F.G. and the 'Ricerca Fondamentale Orientata' (RFO) funding from the University of Bologna to F.G. A.T. contributed to the present publication while attending the PhD programme in Sustainable Development And Climate Change at the University School for Advanced Studies IUSS Pavia, Cycle XXXVIII, with the support of a scholarship financed by the Ministerial Decree no. 351 of 9th April 2022, based on the NRRP - funded by the European Union - NextGenerationEU - Mission 4 "Education and Research", Component 1 "Enhancement of the offer of educational services: from nurseries to universities" - Investment 4.1 "Extension of the number of research doctorates and innovative doctorates for public administration and cultural heritage".

Author contributions

Y.H., X.Z., J.M., J.V., F.G., and A.Z. designed the study. Y.H., K.X., Y.C., and X.Z. sampled the specimens and prepared the materials used for genomic and transcriptomic extraction. Y.H., K.X., Y.C. performed RNA extraction; J.V. performed genome assembly and gene annotations; J.M. performed transposable elements and comparative genomic analyses. A.T. and O.R.S. selected the species and the fossils for divergence time estimation. J.M. and A.T. performed divergence time estimation. O.R.S. and F.G. supervised the analyses. J.M., J.V.

Y.H. and A.T. prepared the figures and supplemental materials. J.M., J.V., A.T., Y.H., F.P., O.R.S., F.G., and A.Z. interpreted the results. J.V., J.M., and Y.H. wrote the first version of the manuscript. All authors critically revised the manuscript.

References

Aguileta G, Hood ME, Refrégier G, Giraud T. 2009. Chapter 3 Genome Evolution in Plant Pathogenic and Symbiotic Fungi. In *Advances in Botanical Research* (ed. Kuete V, Jacquot JP*)*, pp. 151–193. Academic Press, San Diego/London.

Álvarez-Carretero S, Tamuri AU, Battini M, Nascimento FF, Carlisle E, Asher RJ, Yang Z, Donoghue PCJ, dos Reis M. 2022. A species-level timeline of mammal evolution integrating phylogenomic data. *Nature* 602: 263–267.

Andrews S. 2010. FastQC: a quality control tool for high throughput sequence data. http://www.bioinformatics.babraham.ac.uk/projects/fastqc

Benton MJ. Wilf P, Sauquet H. 2022. The Angiosperm Terrestrial Revolution and the origins of modern biodiversity. *New Phytol* 233: 2017–2035.

Bolger, AM, Lohse, M, Usadel, B, 2014. Trimmomatic: a flexible trimmer for Illumina sequence data. *Bioinformatics* 30: 2114–2120.

Bonito G, Smith ME, Nowak M, Healy RA, Guevara G, Cázares E, Kinoshita A, Nouhra ER, Domínguez LS, et al. 2013. Historical Biogeography and Diversification of Truffles in the Tuberaceae and Their Newly Identified Southern Hemisphere Sister Lineage. *PLOS One* 8: e52765.

801 Bonito GM, Smith ME. 2016. General Systematic Position of the Truffles: Evolutionary
802 Theories. In *True Truffle (Tuber* spp.*) in the World*. (ed. Zambonelli, A, Iotti M, Murat C),
803 Soil Biology, vol 47. Springer, Cham.

804 Bourque G, Burns KH, Gehring M, Gorbunova V, Seluanov A, Hammell M, Imbeault M,
805 Izsvák Z, Levin HL, Macfarlan TS, et al. 2018. Ten things you should know about
806 transposable elements. *Genome Biol* 19: 199.

807 Bradshaw MJ, Aime MC, Rokas A, Maust A, Moparthi S, Jellings K, Pane AM, Hendricks
808 D, Pandey B, Li Y, et al. 2023. Extensive intragenomic variation in the internal transcribed
809 spacer region of fungi. *iScience* 26: 107317.

810 Brown MR, PM Gonzalez de La Rosa, Blaxter M. 2025. tidk: a toolkit to rapidly identify
811 telomeric repeats from genomic datasets. *Bioinformatics* 41: btaf049.
812 Brundrett MC, Tedersoo L. 2018. Evolutionary history of mycorrhizal symbioses and global
813 host plant diversity. *New Phytol* 220: 1108–1115.

814 Buchfink B, Xie C, Huson DH. 2015. Fast and sensitive protein alignment using DIAMOND.
815 *Nat Methods* 12: 59–60.

816 Buckley RM, Kortschak RD, Raison JM, Adelson DL. 2017. Similar Evolutionary
817 Trajectories for Retrotransposon Accumulation in Mammals. *Genome Biol Evol* 9: 2336–
818 2353.

819 Capella-Gutiérrez S, Silla-Martínez JM, Gabaldón T. 2009. trimAl: a tool for automated
820 alignment trimming in large-scale phylogenetic analyses. *Bioinformatics* 25: 1972–1973.

821 Carrasco-Valenzuela T, Marino A, Storer JM, Bonnici I, Mazzoni CJ, Fontaine MC, Haudry
822 A, Boulesteix M, Fiston-Lavier A-S. 2025. Manual versus automatic annotation of
823 transposable elements: case studies in *Drosophila melanogaster* and *Aedes albopictus*,

824 balancing accuracy and biological relevance. bioRxiv
825 https://doi.org/10.1101/2025.01.10.632341

826 Castanera R, López-Varas L, Borgognone A, LaButti K, Lapidus A, Schmutz J, Grimwood J,
827 Pérez G, Pisabarro AG, Grigoriev IV, et al. 2016. Transposable Elements versus the Fungal
828 Genome: Impact on Whole-Genome Architecture and Transcriptional Profiles. *PLOS Genet*
829 12: e1006108.

830 Cheng H, Concepcion GT, Feng X. Zhang H, Li H. 2021. Haplotype-resolved de novo
831 assembly using phased assembly graphs with hifiasm. *Nat Methods* 18: 170–175.

832 Cicconardi F, Milanetti E, Pinheiro de Castro EC, Mazo-Vargas A, Van Belleghem SM,
833 Ruggieri AA, Rastas P, Hanly J, Evans E, Jiggins CD et al. 2023. Evolutionary dynamics of
834 genome size and content during the adaptive radiation of Heliconiini butterflies. *Nat Commun*
835 14: 5620.
836 SD. Copley 2020. Evolution of new enzymes by gene duplication and divergence. *FEBS J*
837 287: 1262–1283.

838 Deng X, Liu P, Liu C, Wang Y. 2013. A new white truffle species, *Tuber panzhihuanense*
839 from China. *Mycol Prog* 12: 557–561.

840 dos Reis M, Yang Z. 2019. Bayesian Molecular Clock Dating Using Genome-Scale Datasets.
841 In *Evolutionary Genomics: Statistical and Computational Methods*. (ed. Anisimova M), pp.
842 309–330. Springer, New York.

843 Dyrka W, Lamacchia M, Durrens P, Kobe B, Daskalov A, Paoletti M, Sherman DJ, Saupe SJ.
844 2014. Diversity and Variability of NOD-Like Receptors in Fungi. *Genome Biol Evol*. 6:
845 3137–3158.

Emms DM, Kelly S. 2019. OrthoFinder: phylogenetic orthology inference for comparative genomics. *Genome Biol* 20: 238.

Flynn JM, Hubley R, Goubert C, Rosen J, Clark AG, Feschotte C, Smit AF. 2020. RepeatModeler2 for automated genomic discovery of transposable element families. *Proc Natl Acad Sci USA* 117: 9451–9457.

Fouché S, Badet T, Oggenfuss U, Plissonneau C, Francisco CS, Croll D. 2020. Stress-Driven Transposable Element De-repression Dynamics and Virulence Evolution in a Fungal Pathogen. *Mol Biol Evol* 37: 221–239.

Galagan JE, Selker EU. 2004. RIP: the evolutionary cost of genome defense. *Trends Genet* 20: 417–423.

Ganley ARD, Kobayashi T. 2011. Monitoring the Rate and Dynamics of Concerted Evolution in the Ribosomal DNA Repeats of Saccharomyces cerevisiae Using Experimental Evolution. *Mol Biol Evol* 28: 2883–2891.

Gao X, Hou Y, Ebina H, Levin HL, Voytas DF. 2008. Chromodomains direct integration of retrotransposons to heterochromatin. *Genome Res* 18: 359–369.

Garcia S, Kovarik A, Maiwald S, Mann L, Schmidt N, Pascual-Díaz JP, Vitales D, Weber B, Heitkam T. 2024. The Dynamic Interplay Between Ribosomal DNA and Transposable Elements: A Perspective From Genomics and Cytogenetics. *Mol Biol Evol* 41: msae025

Goubert C, Craig RJ, Bilat AF, Peona V, Vogan AA, Protasio AV. 2022. A beginner's guide to manual curation of transposable elements. *Mob DNA* 13: 7.

Grabherr MG, Haas BJ, Yassour M, Levin JZ, Thompson DA, Amit I, Adiconis X, Fan L, Raychowdhury R, Zeng Q, et al. 2011. Full-length transcriptome assembly from RNA-seq data without a reference genome. *Nat Biotechnol* 29: 644-52.

869 Graziosi S, Puliga F, Iotti M, Amicucci A, Zambonelli A. 2024. In vitro interactions between
870 *Bradyrhizobium* spp. and *Tuber magnatum* mycelium. *Environ Microbiol Rep* 16(3): e13271.

871 Hagberg A, Swart PJ, Schult DA. 2008. Exploring Network Structure, Dynamics, and
872 Function using NetworkX. Proceedings of the 7th Python in Science Conference (SciPy
873 2008) United States.

874 Han M, Wang Q, Baiyintala, Wuhanqimuge. 2019. The whole-genome sequence analysis of
875 *Morchella sextelata*. *Sci Rep* 9: 15376.

876 Hane JK, Rouxel T, Howlett BJ, Kema GH, Goodwin SB, Oliver RP. 2011. A novel mode of
877 chromosomal evolution peculiar to filamentous Ascomycete fungi. *Genome Biol* 12: R45.

878 Hiltunen M, Ament-Velásquez SL, Johannesson H. 2021. The Assembled and Annotated
879 Genome of the Fairy-Ring Fungus *Marasmius oreades*. *Genome Biol Evol* 13: evab126.

880 Hoang DT, Chernomor O, von Haeseler A, Minh BQ, Vinh LS. 2018. UFBoot2: Improving
881 the Ultrafast Bootstrap Approximation. *Mol Biol Evol* 35: 518–522.

882 Hori Y, Shimamoto A, Kobayashi T. 2021. The human ribosomal DNA array is composed of
883 highly homogenized tandem clusters. *Genome Res* 31: 1971–1982.

884 Hori Y, Engel C, Kobayashi T. 2024. Regulation of ribosomal RNA gene copy number,
885 transcription and nucleolus organization in eukaryotes. *Nat Rev Mol Cell Biol* 24: 414–429.

886 Iyer LM, Zhang D, de Souza RF, Pukkila PJ, Rao A, Aravind L. 2014. Lineage-specific
887 expansions of TET/JBP genes and a new class of DNA transposons shape fungal genomic
888 and epigenetic landscapes. *Proc Natl Acad Sci USA* 111: 1676–1683.

889 Jarvis ED, Mirarab S, Aberer AJ, Li B, Houde P, Li C, Ho SYW, Faircloth BC, Nabholz B,
890 Howard JT, et al. 2014. Whole-genome analyses resolve early branches in the tree of life of
891 modern birds. *Science* 346: 1320–1331.

892 Jones P, Binns D, Chang HY, Fraser M, Li W, McAnulla C, McWilliam H, Maslen J,
893 Mitchell A, Nuka G, et al. 2014. InterProScan 5: genome-scale protein function
894 classification. *Bioinformatics* 30: 1236–1240.

895 Kalyaanamoorthy S, Minh BQ, Wong TKF, von Haeseler A, Jermiin LS. 2017. ModelFinder:
896 fast model selection for accurate phylogenetic estimates. *Nat Methods* 14: 587–589.

897 Katoh K, Standley DM. 2013. MAFFT Multiple Sequence Alignment Software Version 7:
898 Improvements in Performance and Usability. *Mol Biol Evol* 30: 772–780.

899 Kent TV, Uzunović J, Wright SI. 2017. Coevolution between transposable elements and
900 recombination. *Philos Trans R Soc B Biol Sci* 372: 20160458.

901 Kim JH, Nagaraja R, Ogurtsov AY, Noskov VN, Liskovykh M, Lee H-S, Hori Y, Kobayashi
902 T, Hunter K, Schlessinger D et al. 2024. Comparative analysis and classification of highly
903 divergent mouse rDNA units based on their intergenic spacer (IGS) variability. *NAR Genom*
904 *Bioinform* 6: lqae070.

905 Kohler A, Kuo A, Nagy L, Morin E, Barry KW, Buscot F, Canbäck B, Choi C, Cichocki N,
906 Clum A *et al.* 2015. Convergent losses of decay mechanisms and rapid turnover of symbiosis
907 genes in mycorrhizal mutualists. *Nat Genet* 47: 410–415

908 Korf I. 2004. Gene finding in novel Genomes. *BMC Bioinformatics* 5: 59.

909 Laetsch DR, Blaxter ML. 2017. BlobTools: Interrogation of genome assemblies [version1;
910 peer review: 2 approved with reservations]. *F1000Research* 6: 1287.

911 Lagesen K, Hallin P, Rødland EA, Stærfeldt HH, Rognes T, Ussery DW. 2007. RNAmmer:
912 consistent and rapid annotation of ribosomal RNA genes. *Nucleic Acids Res* 35: 3100–3108.

913 Lemmond B, Sow A, Bonito G, Smith ME. 2023. Accidental cultivation of the European
914 truffle *Tuber brumale* in North American truffle orchards. *Mycorrhiza* 33: 221–228.

915 Leonardi P, Baroni R, Puliga F, Iotti M, Salerni E, Perini C, Zambonelli A. 2021. Co-
916 occurrence of true truffle mycelia in *Tuber magnatum* fruiting sites. *Mycorrhiza* 31: 389–394.

917 Li H. 2018. minimap2: pairwise alignment for nucleotide sequences. *Bioinformatics* 34:
918 3094–3100.

919 Llorens C, Futami R, Covelli L, Domínguez-Escribá L, Viu JM, Tamarit D, Aguilar-
920 Rodríguez J, Vicente-Ripolles M, Fuster G, Bernet GP, et al. 2011. The Gypsy Database
921 (GyDB) of mobile genetic elements: release 2.0. *Nucleic Acids Res* 39: 70–74.

922 Lomsadze A, Ter-Hovhannisyan V, Chernoff YO, Borodovsky M. 2005. Gene identification
923 in novel eukaryotic genomes by self-training algorithm. *Nucleic Acids Res* 33: 6494–6506.

924 Lovell JT, Sreedasyam A, Schranz ME, Wilson M, Carlson JW, Harkess A, Emms D,
925 Goodstein DM, Schmutz J. 2022. GENESPACE tracks regions of interest and gene copy
926 number variation across multiple genomes. *eLife* 11 :e78526.

927 Majoros WH, Pertea M, Salzberg SL. 2004. TigrScan and GlimmerHMM: two open-source
928 ab initio eukaryotic gene-finders. *Bioinformatics* 20: 2878-2879.

929 Mapleson D, Garcia Accinelli G, Kettleborough G, Wright J, Clavijo BJ. 2017. KAT: a *k*-mer
930 analysis toolkit to quality control NGS datasets and genome assemblies. *Bioinformatics* 33:
931 574–576.

Marín I, Lloréns C. 2000. Ty3/Gypsy Retrotransposons: Description of New Arabidopsis thaliana Elements and Evolutionary Perspectives Derived from Comparative Genomic Data. *Mol Biol Evo*l 17: 1040–1049.

Martelossi J, Iannello M, Ghiselli F, Luchetti A. 2024. Widespread HCD-tRNA derived SINEs in bivalves rely on multiple LINE partners and accumulate in genic regions. *Mob DNA*15: 22.

Martin F, Aerts A, Ahrén D, Brun A, Danchin EGJ, Duchaussoy F, Gibon J, Kohler A, Lindquist E, Pereda V, et al. 2008. The genome of *Laccaria bicolor* provides insights into mycorrhizal symbiosis. *Nature* 452: 88–92.

Martin F, Kohler A, Murat C, Balestrini R, Coutinho PM, Jaillon O, Montanini B, Morin E, Noel B, Percudani R, et al. 2010. Périgord black truffle genome uncovers evolutionary origins and mechanisms of symbiosis. *Nature* 464: 1033–1038.

Martin, F., Tunlid, A. (2009). The Ectomycorrhizal Symbiosis: a Marriage of Convenience. In *Plant Relationships* (ed. Deising HB). The Mycota, vol 5, pp. 237-257. Springer, Berlin, Heidelberg.

Mello A, Murat C, Bonfante P. 2006. Truffles: much more than a prized and local fungal delicacy. *FEMS Microbiol Lett* 260: 1–8.

Mendes FK, Vanderpool D, Fulton B, Hahn MW. 2020. CAFE 5 models variation in evolutionary rates among gene families. *Bioinformatics* 36:5516–5518.

Minh BQ, Schmidt HA, Chernomor O, Schrempf D, Woodhams MD, Von Haeseler A, Lanfear R. 2020. IQ-TREE 2: new models and efficient methods for phylogenetic inference in the genomic era. *Mol biol evol* 37: 1530–1534.

954 Mistry J, Chuguransky S, Williams L, Qureshi M, Salazar GA, Sonnhammer ELL, Tosatto
955 SCE, Paladin L, Raj S, Richardson LJ, et al. 2021. Pfam: The protein families database in
956 2021. *Nucleic Acids Res* 49: 412–419.

957 Miyauchi S, Kiss E, Kuo A, Drula E, Kohler A, Sánchez-García M, Morin E, Andreopoulos
958 B, Barry KW, Bonito G, et al. 2020. Large-scale genome sequencing of mycorrhizal fungi
959 provides insights into the early evolution of symbiotic traits. *Nat Commun* 11: 5125.

960 Monaco P, Naclerio G, Mello A and Bucci A. 2022. Role and potentialities of bacteria
961 associated with *Tuber magnatum*: A mini-review.
962 *Front Microbiol* 13: 1017089.

963 Montagna M, Tong KJ, Magoga G, Strada, Tintori A, Ho SYW, Lo N. 2019. Recalibration
964 of the insect evolutionary time scale using Monte San Giorgio fossils suggests survival of key
965 lineages through the End-Permian Extinction. *Proc R Soc B* 286: 20191854.

966 Montanini B, Chen PY, Morselli M, Jaroszewicz A, Lopez D, Martin F, Ottonello S,
967 Pellegrini M. 2014. Non-exhaustive DNA methylation-mediated transposon silencing in the
968 black truffle genome, a complex fungal genome with massive repeat element content.
969 *Genome Biol* 15: 411.

970 Mosè M, Berkeley MR, Seppey M, Simão FA, Zdobnov EM. 2021. BUSCO Update: Novel
971 and Streamlined Workflows along with Broader and Deeper Phylogenetic Coverage for
972 Scoring of Eukaryotic, Prokaryotic, and Viral Genomes. *Mol Biol Evol* 38: 4647–4654.

973 Murat C, Kuo A, Barry KW, Clum A, Dockter RB, Fauchery L, Iotti M, Kohler A, LaButti
974 K, Lindquist EA, et al. 2018. Draft Genome Sequence of *Tuber borchii* Vittad., a Whitish
975 Edible Truffle. Genome Announc 6, e00537-18.

976 Murat C, Payen T, Noel B, Kuo A, Morin E, Chen J, Kohler A, Krizsán K, Balestrini R, Da
977 Silva C, et al. 2018. Pezizomycetes genomes reveal the molecular basis of ectomycorrhizal
978 truffle lifestyle. *Nat Ecol Evol* 2: 1956–1965.

979 Muszewska A, Steczkiewicz K, Stepniewska-Dziubinska M, Ginalski K. 2019. Transposable
980 elements contribute to fungal genes and impact fungal lifestyle. *Sci Rep* 9: 4307.

981 Neumann P, Navrátilová A, Koblížková A, Kejnovský E, Hřibová E, Hobza R, Widmer A,
982 Doležel J, Macas J. 2011. Plant centromeric retrotransposons: a structural and cytogenetic
983 perspective. *Mob DNA* 2: 4.

984 Novikova O, Smyshlyaev G, Blinov A. 2010. Evolutionary genomics revealed interkingdom
985 distribution of Tcn1-like chromodomain-containing Gypsy LTR retrotransposons among
986 fungi and plants. *BMC Genomics* 11: 231.

987 Oggenfuss U, Badet T, Wicker T, Hartmann FE, Singh NK, Abraham L, Karisto P,
988 Vonlanthen T, Mundt C, McDonald BA, et al. 2021. A population-level invasion by
989 transposable elements triggers genome expansion in a fungal pathogen. *eLife* 1: e69249.

990 Pagel M. 1999. Inferring the historical patterns of biological evolution. *Nature* 401: 877–884.

991 Palmer J, Stajich J. 2019. nextgenusfs/funannotate: funannotate v1.5.3. Zenodo.

992 Paradis E, Claude J, Strimmer K. 2004. APE: Analyses of Phylogenetics and Evolution in R
993 language. *Bioinformatics* 20 :289–290.

994 Payen T, Murat C, Martin FM. 2016. Reconstructing the evolutionary history of gypsy
995 retrotransposons in the Périgord black truffle (*Tuber melanosporum* Vittad.). *Mycorrhiza*
996 26 : 553–563.

997 Pellegrin C, Morin E, Martin FM, Veneault-Fourrey C. 2015. Comparative Analysis of
998 Secretomes from Ectomycorrhizal Fungi with an Emphasis on Small-Secreted Proteins. *Front*
999 *Microbiol* 6: 1278.

1000 Peona V, Blom MPK, Xu L, Burri R, Sullivan S, Bunikis I, Liachko I, Haryoko T, Jønsson
1001 KA, Zhou Q, et al. 2021. Identifying the causes and consequences of assembly gaps using a
1002 multiplatform genome assembly of a bird-of-paradise. *Mol Ecol Resour* 21: 263–286.

1003 Peona V, Martelossi J, Almojil D, Bocharkina J, Brännström I, Brown M, Cang A, Carrasco-
1004 Valenzuela T, DeVries J, Doellman M, et al. 2024. Teaching transposon classification as a
1005 means to crowd source the curation of repeat annotation – a tardigrade perspective. *Mob DNA*
1006 15: 10.

1007 Poma A, Pacioni G, Ranalli R, Miranda M. 1998. Ploidy and chromosomal number in *Tuber*
1008 *aestivum*. *FEMS Microbiol Lett* 167: 101–105

1009 Poma A, Venora G, Miranda M, Pacioni G. 2002. The karyotypes of three *Tuber* species
1010 (Pezizales, Ascomycota). *Caryologia 55:* 307–313.

1011 Price MN, Dehal PS, Arkin AP. 2010. FastTree 2 – Approximately Maximum-Likelihood
1012 Trees for Large Alignments. *PLoS One* 5: e9490.

1013 Quinlan AR, Hall IM. 2010. BEDTools: a flexible suite of utilities for comparing genomic
1014 features. *Bioinformatics* 26: 841–842.

1015 R Core Team. 2021. R: A Language and Environment for Statistical Computing. R
1016 Foundation for Statistical Computing, Vienna.

1017 Raffaele S, Farrer RA, Cano LM, Studholme DJ, MacLean D, Thines M, Jiang RHY, Zody
1018 MC, Kunjeti SG, Donofrio NM, et al. 2010. Genome Evolution Following Host Jumps in the
1019 Irish Potato Famine Pathogen Lineage. *Science* 330: 1540–1543.

1020 Rajashekar B, Kohler A, Johansson T, Martin F, Tunlid A, Ahrén D. 2009. Expansion of
1021 signal pathways in the ectomycorrhizal fungus *Laccaria bicolor* – evolution of nucleotide
1022 sequences and expression patterns in families of protein kinases and RAS small GTPases.
1023 *New Phytol* 183: 365–379.

1024 Rambaut A, Drummond AJ, Xie D, Baele G, Suchard MA. 2018. Posterior Summarization in
1025 Bayesian Phylogenetics Using Tracer 1.7. *Syst Biol* 67: 901–904.

1026 Ramírez-Barahona S, Sauquet H, Magallón S. 2020. The delayed and geographically
1027 heterogeneous diversification of flowering plant families. *Nat Ecol Evol* 4: 1232–1238.

1028 Ranallo-Benavidez TR, Jaron KS, Schatz MC. 2020. GenomeScope 2.0 and Smudgeplot for
1029 reference-free profiling of polyploid genomes. *Nat Commun* 11: 1432.

1030 Revell LJ. 2024. phytools 2.0: an updated R ecosystem for phylogenetic comparative
1031 methods (and other things). *PeerJ* 12:e16505.

1032 Rhie A, McCarthy SA, Fedrigo O, Damas J, Formenti G, Koren S, Uliano-Silva M, Chow W,
1033 Fungtammasan A, Kim J, et al. 2021. Towards complete and error-free genome assemblies of
1034 all vertebrate species. *Nature* 592: 737–746.

1035 Rhie A, Walenz BP, Koren S, Phillippy AM. 2020. Merqury: reference-free quality,
1036 completeness, and phasing assessment for genome assemblies. *Genome Biol* 21: 245.

1037 Riccioni C, Rubini A, Belfiori B, Passeri V, Paolocci F, Arcioni S. 2008. Tmt1: the first
1038 LTR-retrotransposon from a *Tuber* spp.. *Curr Genet* 53: 23–34.

1039 Robicheau BM, Susko E, Harrigan AM, Snyder M. 2017. Ribosomal RNA Genes Contribute
1040 to the Formation of Pseudogenes and Junk DNA in the Human Genome. *Genome Biol Evol* 9:
1041 380–397

1042 Ruggieri AA, Livraghi L, Lewis JJ, Evans E, Cicconardi F, Hebberecht L, Ortiz-Ruiz Y,
1043 Montgomery SH, Ghezzi A, Rodriguez-Martinez JA, et al. 2022. A butterfly pan-genome
1044 reveals that a large amount of structural variation underlies the evolution of chromatin
1045 accessibility. *Genome Res* 32: 1862–1875.

1046 Sato H. 2024. The evolution of ectomycorrhizal symbiosis in the Late Cretaceous is a key
1047 driver of explosive diversification in Agaricomycetes. *New Phytol* 241: 444–460.

1048 Schaack S, Gilbert C, Feschotte C. 2010. Promiscuous DNA: horizontal transfer of
1049 transposable elements and why it matters for eukaryotic evolution. *Trends Ecol Evol* 25: 537–
1050 546.

1051 Schmidt SM, Houterman PM, Schreiver I, Ma L, Amyotte S, Chellappan B, Boeren S,
1052 Takken FLW, Rep M. 2013. MITEs in the promoters of effector genes allow prediction of
1053 novel virulence genes in *Fusarium oxysporum*. *BMC Genomics* 14: 119.

1054 Smit AFA, Hubley R, Green P. 2013-2015. RepeatMasker Open-4.0.
1055 http://www.repeatmasker.org

1056 Stanke M, Diekhans M, BaertschR, Haussler D. 2008. Using native and syntenically mapped
1057 cDNA alignments to improve *de novo* gene finding. *Bioinformatics* 24: 637–644.

1058 Sundaram S, Kim SJ, Suzuki H, Mcquattie CJ, Hiremath ST, Podila GK. 2001. Isolation and
1059 Characterization of a Symbiosis-Regulated ras from the Ectomycorrhizal Fungus *Laccaria*
1060 *bicolor*. *Mol Plant Microbe Interact* 14: 618–628.

1061 Tedersoo L, May TW, Smith ME. 2010. Ectomycorrhizal lifestyle in fungi: global diversity,
1062 distribution, and evolution of phylogenetic lineages. *Mycorrhiza* 20: 217–263.

1063 Testa AC, Hane JK, Ellwood SR, Oliver RP. 2015. CodingQuarry: highly accurate hidden
1064 Markov model gene prediction in fungal genomes using RNA-seq transcripts. *BMC*
1065 *Genomics* 16: 170.

1066 Thon MR, Pan H, Diener S, Papalas J, Taro A, Mitchell TK, Dean RA. 2006. The role of
1067 transposable element clusters in genome evolution and loss of synteny in the rice blast fungus
1068 *Magnaporthe oryzae*. *Genome Biol*. 7: R16.

1069 To TH, Jung M, Lycett S, Gascuel O. 2016. Fast Dating Using Least-Squares Criteria and
1070 Algorithms. *Syst Biol* 65: 82–97.

1071 Treindl AD, Stapley J, Winter DJ, Cox MP, Leuchtmann A. 2021. Chromosome-level
1072 genomes provide insights into genome evolution, organization and size in Epichloe fungi.
1073 *Genomics* 113: 4267–4275.

1074 Tumescheit C, Firth AE, Brown K. 2022. CIAlign: A highly customisable command line tool
1075 to clean, interpret and visualise multiple sequence alignments. *PeerJ* 10: e12983.

1076 Wan S, Zheng Y, Tang L, Wang R, Liu P, Yu F. 2015. Diversity of culturable bacteria
1077 associated with *Tuber panzhihuanense-Pinus armandii* ectomycorrhizosphere soil. *Plant*
1078 *Divers* 37: 861-870.

1079 Wicker T, Sabot F, Hua-Van A, Bennetzen JL, Capy P, Chalhoub B, Flavell A, Leroy P,
1080 Morgante M, Panaud O, et al. 2007. A unified classification system for eukaryotic
1081 transposable elements. *Nat Rev Genet* 8: 973–982.

1082 Wong WY, Simakov O. 2019. RepeatCraft: a meta-pipeline for repetitive element de-
1083 fragmentation and annotation. *Bioinformatics* 35:1051–1052.

1084 Wood DE, Lu J, Langmead B. 2019. Improved metagenomic analysis with Kraken 2.
1085 *Genome Biol* 20: 257.

Yang K, Tian J, Keller NP. 2022. Post-translational modifications drive secondary metabolite biosynthesis in *Aspergillus*: a review. *Environ Microbiol* 24: 2857-–2881

Yao Y, Wei J, Zhuang W, Wei T, Li Y, Wei X, Deng H, Liu D, Cai L, Li J, et al. 2020. Threatened species list of China's macrofungi. *Biodivers Sci* 28: 20–25.

Yashiroda H, Tanaka K. 2003. But1 and But2 proteins bind to Uba3, a catalytic subunit of E1 for neddylation, in fission yeast. *Biochem Biophys Res Commun* 311: 691–695.

Zheng J, Ge Q, Yan Y, Zhang X, Huang L, Yin Y. 2023. dbCAN3: automated carbohydrate-active enzyme and substrate annotation. *Nucleic Acids Res* 51: 115–121.

Zhuang W, Li Y, Zheng H, Zeng Z, Wang X. 2020. Threat status of non-lichenized macro-ascomycetes in China and its threatening factors. *Biodiver Sci* 28: 26–40.

Figure legends

Fig. 1: A highly compartmentalised genome colonised by Chromoviridae-related Gypsy transposons. **(A)** From outer to inner circles: distribution of transposons, genes, TE hotspots, and TE coldspots across the 17 main contigs of the *T. panzhihuanense* nuclear genome. **(B)** Correlation between TE density against gene density across 50 kb non-overlapping genomic windows; rho = Spearman's rank correlation coefficient. **(C)** Phylogenetic tree of representative Gypsy RT protein segments longer than 100 amino acids. Green circles highlight crown nodes of identified families with bootstrap support values ≥ 75. **(D)** Genomic occurrence of the four identified Gypsy clades in the *T. panzhihuanense* genome.

Fig 2: Genomic features of rDNA loci. (A) Genomic locations of nuclear rDNA genes. The size of contigs is proportional to their length, but different scales are used for contigs ctg_1 to ctg_17, and ctg_19 to ctg_29. The length of each contig is reported below its name. **(B)** Self-alignment of ctg_19 as an example of the 45S rDNA locus structure. **(C)** Simplified structure

of 45S rDNA loci; the length of blocks is not proportional to their actual length. IR = inverted repeat, DR = direct repeat, IGS = intergenic spacer, ITS1 and ITS2 = internal transcribed spacers. **(D)** Alignment of 45S rDNA loci from 18S to 28S. Red lines highlight nucleotides that differ from the consensus sequence. The names of each locus reflect the naming system used in panel A. **(E)** Same as (**D**), but for 5S rDNA genes.

Fig. 3: Late Cretaceous emergence of Tuberaceae and a Paleogene diversification of true truffles. Phylogenetic relationships and divergence time estimations obtained with 1,057 complete and single-copy BUSCO genes. The species tree was constructed using an amino acid supermatrix, while both protein (black) and nucleotide (red) data were used for divergence time estimation. All nodes received maximum support values from the species tree inference, except for the split between *Arthrobotrys* and Pezizomycetes. The outgroup *Schizosaccharomyces osmophilus* was removed for visualisation purposes. Numbers within circles represent the calibration points described in supplementary table S11. Ne=Neoproterozoic, Cam=Cambrian, Or=Ordovician, Si=Silurian, De=Devonian, Car=Carboniferous, Pe=Permian, Tr=Triassic, Ju=Jurassic, Cr=Cretaceous, Pa=Paleogene.

Fig. 4: Lineage-specific proliferation of different Gypsy clades drives genome expansion in Tuberaceae. Correlations between **(A)** total TE content and **(B)** Gypsy content with assembly size, used as a proxy for genome size after correcting for shared evolutionary history using phylogenetic independent contrasts (PIC). **(C)** Assembly size and TE content for 13 Pezizales species used in comparative genomic analyses. **(D)** Relative contribution of identified clades to the total Gypsy content of Tuberaceae. Others referred to Gypsy clades that were not identified and characterised in *T. panzhihuanense*. **(E)** Repeat landscape profile describing the activity over time of Gypsy clades in the *T. panzhihuanense* genome after transforming the CpG-corrected Kimura distance into millions of years using a substitution rate of 3.36×10^{-3} per million year. The green box highlights the mean divergence time

between *T. panzhihuanense* from *T. borchii* based on nucleotides (lower bound) and amino acids (upper bound). **(F)** Clade-specific phylogenetic trees of all Gypsy RT segments with a length of at least 100 amino acids extracted from all Tuberaceae genomes. Different colours highlight different species. All species abbreviations are reported in Fig. 3

Fig. 5: High gene family turnover rates within Tuberaceae and synteny conservation with Morchellaceae. **(A)** Gene family expansions and contractions along the Pezizales phylogeny. At each node, the top number indicates the number of gene family expansions, while the bottom number indicates the number of contractions. The numbers in parentheses represent the significantly expanded and contracted gene families. λ = birth-death model rates fitted with CAFE for Tuberaceae and all other Pezizales species. Species abbreviations are shown in Fig. 3. **(B)** Syntenic relationships between the *T. panzhihuanense* and *M. sextelata* genomes. The length of syntenic blocks is proportional to their actual length in base pairs. **(C)** and **(D)** Examples of syntenic genomic regions between *T. panzhihuanense* and *M. sextelata* involved in gene loss and small-scale rearrangements. Private genes = genes without any known orthologous relationship. Blocks have different scales and are shown at the bottom. **(E)** Cumulative distribution of the length of syntenic blocks in *T. panzhihuanense* and *M. sextelata*. **(F)** and **(G)** Comparison of TE and gene coverage (% of base pairs) across syntenic and non-syntenic genomic regions in *T. panzhihuanense*, calculated over non-overlapping genomic windows of 50 kb. Non-syntenic genomic regions were found to be significantly more TE-rich and less gene dense (Wilcoxon rank-sum test, $p < 0.01$). **(H)** TE coverage (% of base pairs) across exons, introns, and 5 kb of gene-flanking regions for genes belonging to significantly expanded gene families identified in the branch leading to Tuberaceae diversification, as well as in the *T. panzhihuanense* terminal branch, compared to all other genes. Genes belonging to significantly expanded gene families were found to be

significantly more TE-rich across all genomic compartments (Wilcoxon rank-sum test, $p < 0.01$).

Fig. 6: Ancestral gene duplications of ECM-induced gene families. **(A)** CAFE results for three ectomycorrhizal (ECM)–induced gene families that are significantly expanded on the stem branch of Tuberaceae. For each node, inferred and observed gene family counts are shown on internal and terminal branches, respectively. Green indicates expansions, red indicates contractions, and significant changes are marked with an asterisk. Numbers in brackets indicate node IDs and refer to Supplemental Table S8. Species abbreviations are given in Fig. 3. **(B)** InterProScan domain annotations of representative *T. panzhihuanense* proteins from each of the three gene families. For OG0000075, we used a reference protein from *T. magnatum* because no family members were detected in *T. panzhihuanense*. Symbols correspond to those in (A). TPR, tetratricopeptide repeat. Supplemental Fig. S17 shows the results for the two others significantly expanded ECM-induced gene families, OG0000009 and OG0000138, encoding ankyrin repeat–containing proteins and AAA ATPases, respectively.

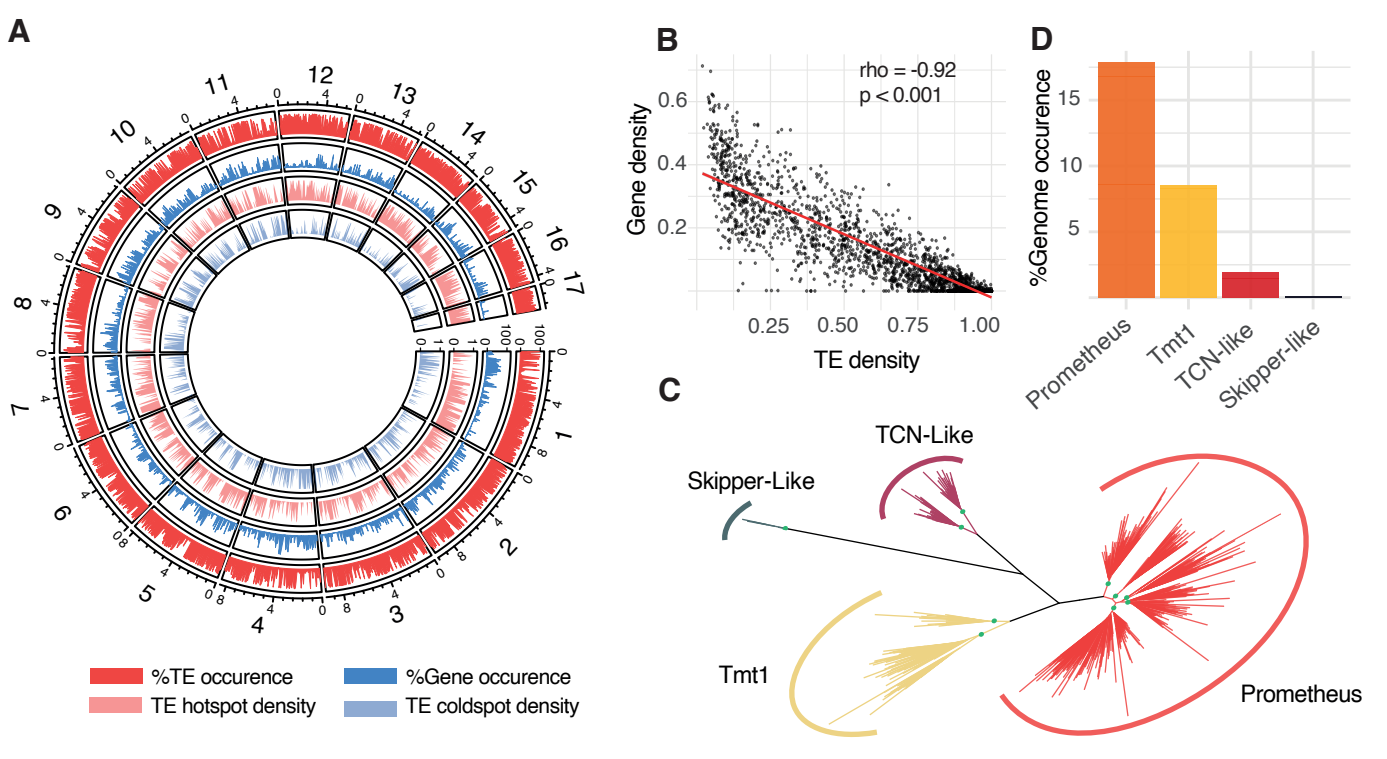
A
%TE occurence
TE hotspot density
%Gene occurence
TE coldspot density
B
rho = -0.92
p < 0.001
Gene density
TE density
0.2
0.4
0.6
0.25
0.50
0.75
1.00
D
%Genome occurence
5
10
15
Prometheus
Tmt1
TCN-like
Skipper-like
C
TCN-Like
Skipper-Like
Tmt1
Prometheus

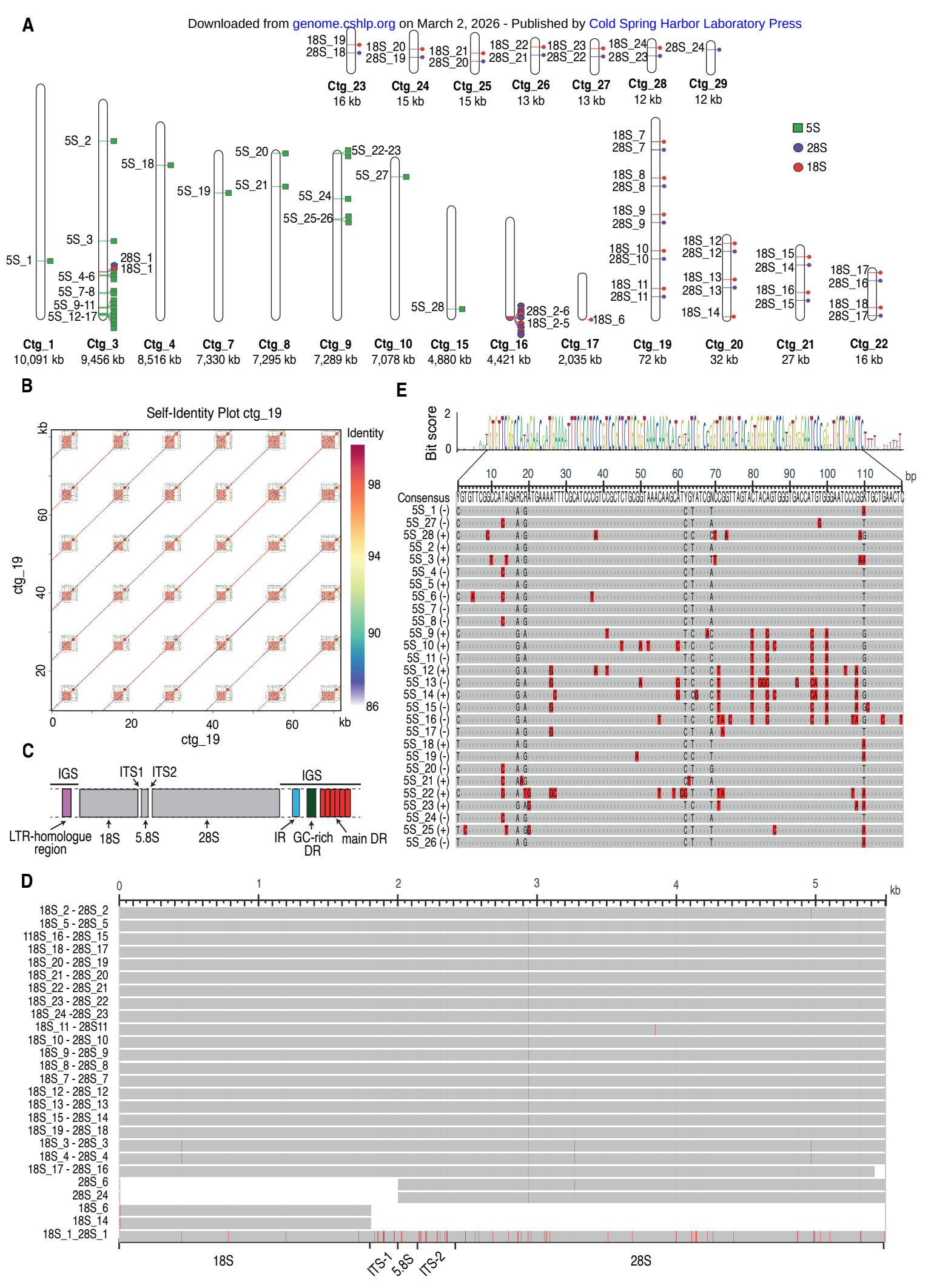

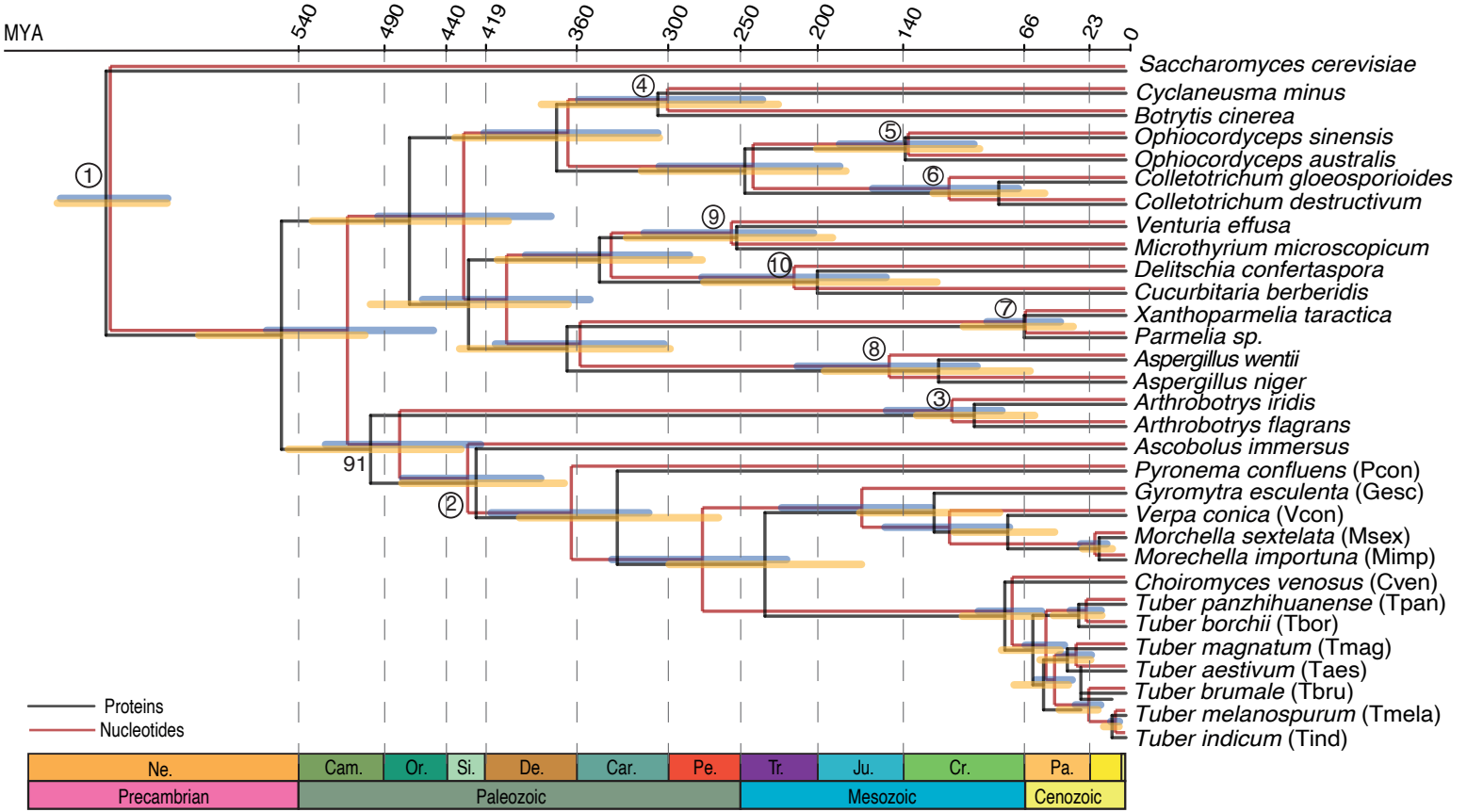
MYA
540
490
440
419
360
300
250
200
140
66
23
0
Saccharomyces cerevisiae
Cyclaneusma minus
Botrytis cinerea
Ophiocordyceps sinensis
Ophiocordyceps australis
Colletotrichum gloeosporioides
Colletotrichum destructivum
Venturia effusa
Microthyrium microscopicum
Delitschia confertaspora
Cucurbitaria berberidis
Xanthoparmelia taractica
Parmelia sp.
Aspergillus wentii
Aspergillus niger
Arthrobotrys iridis
Arthrobotrys flagrans
Ascobolus immersus
Pyronema confluens (Pcon)
Gyromytra esculenta (Gesc)
Verpa conica (Vcon)
Morchella sextelata (Msex)
Morechella importuna (Mimp)
Choiromyces venosus (Cven)
Tuber panzhihuanense (Tpan)
Tuber borchii (Tbor)
Tuber magnatum (Tmag)
Tuber aestivum (Taes)
Tuber brumale (Tbru)
Tuber melanospurum (Tmela)
Tuber indicum (Tind)
①
②
③
④
⑤
⑥
⑦
⑧
⑨
⑩
91
Proteins
Nucleotides
Ne.
Cam.
Or.
Si.
De.
Car.
Pe.
Tr.
Ju.
Cr.
Pa.
Precambrian
Paleozoic
Mesozoic
Cenozoic

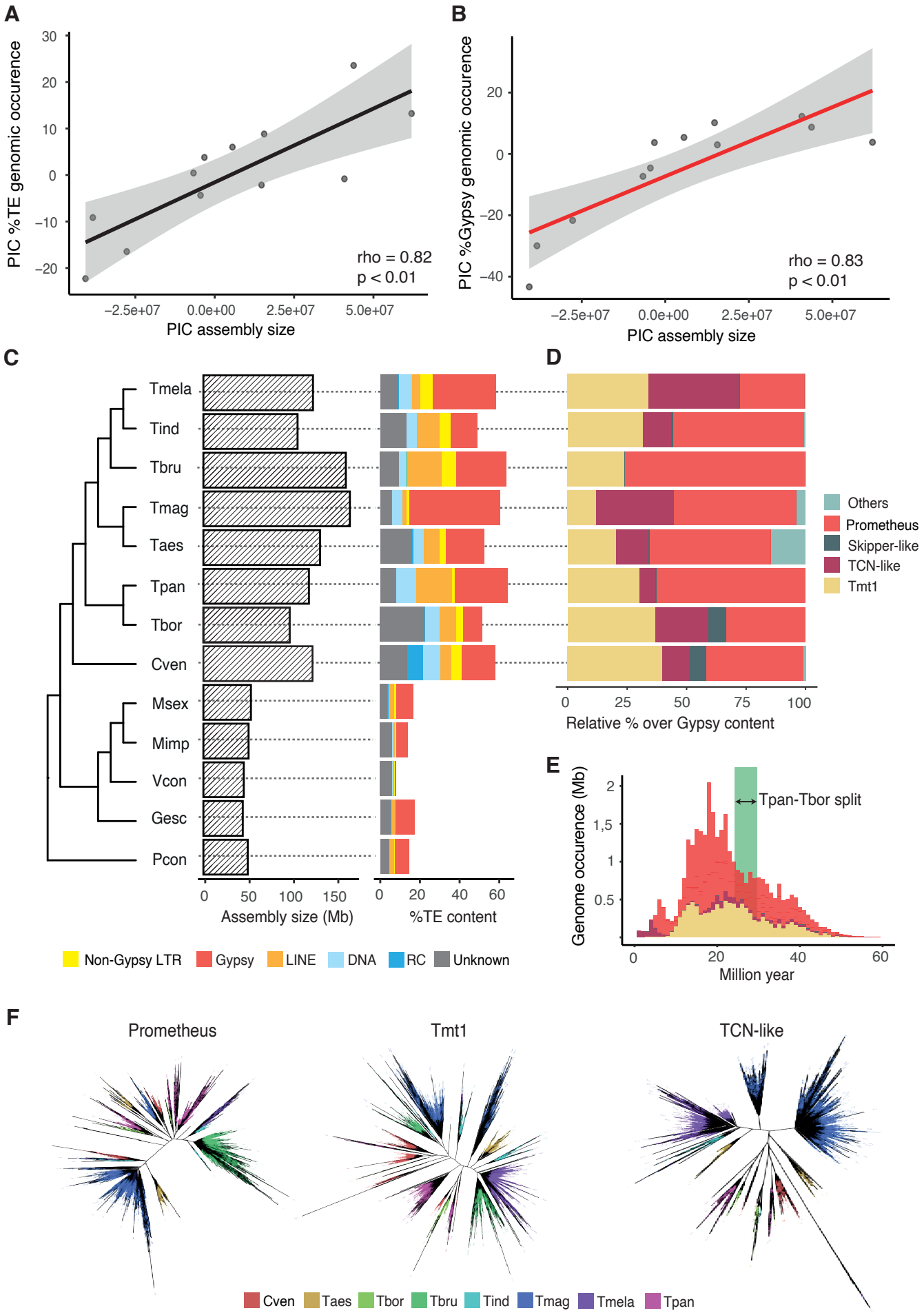
A
PIC %TE genomic occurence
PIC assembly size
rho = 0.82
p < 0.01
B
PIC %Gypsy genomic occurence
PIC assembly size
rho = 0.83
p < 0.01
C
Tmela
Tind
Tbru
Tmag
Taes
Tpan
Tbor
Cven
Msex
Mimp
Vcon
Gesc
Pcon
Assembly size (Mb)
%TE content
Non-Gypsy LTR
Gypsy
LINE
DNA
RC
Unknown
D
Others
Prometheus
Skipper-like
TCN-like
Tmt1
Relative % over Gypsy content
E
Genome occurence (Mb)
Tpan-Tbor split
Million year
F
Prometheus
Tmt1
TCN-like
Cven
Taes
Tbor
Tbru
Tind
Tmag
Tmela
Tpan

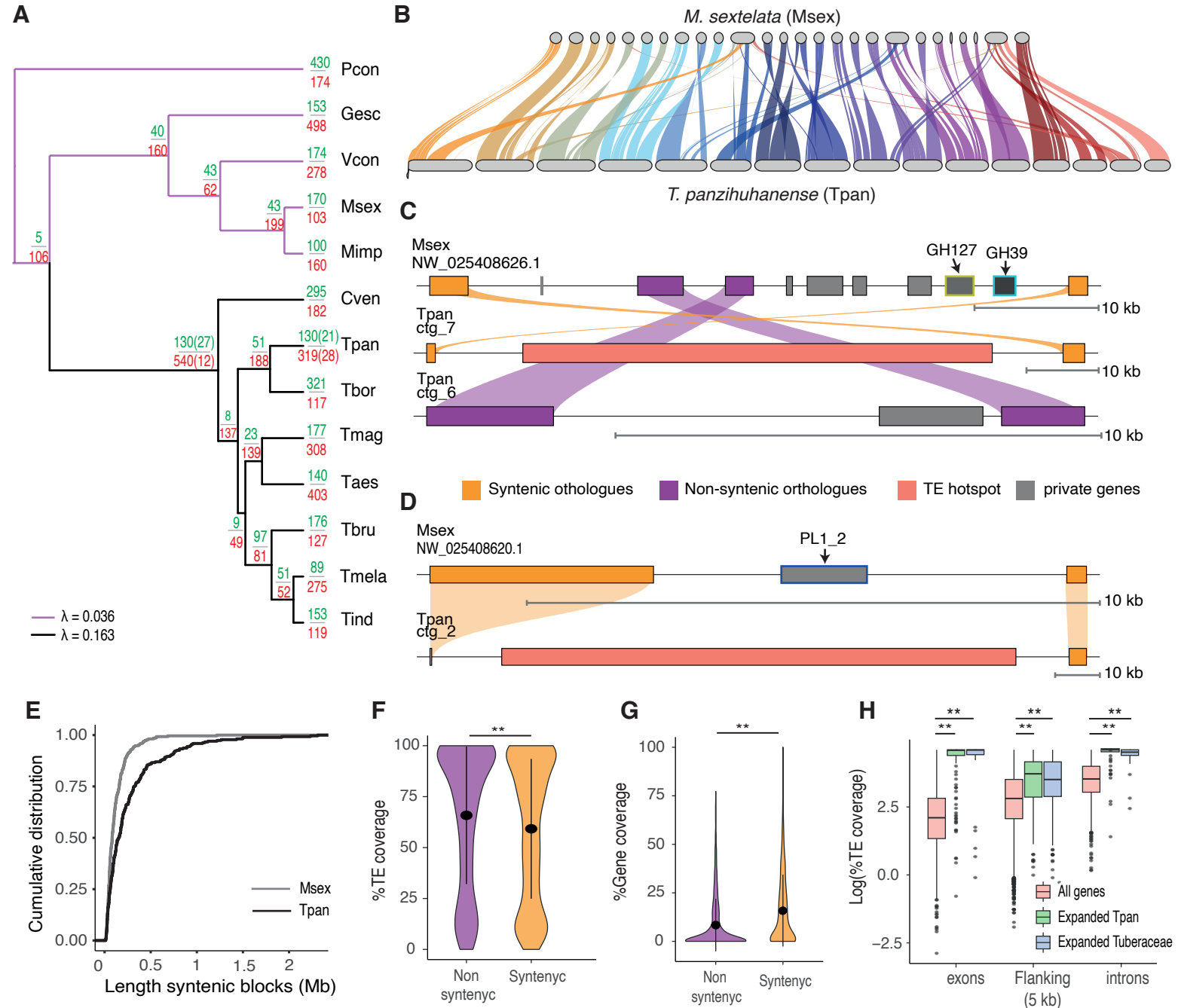
A
430
174
Pcon
153
498
Gesc
40
160
174
278
Vcon
43
62
170
103
Msex
43
199
100
160
Mimp
5
106
295
182
Cven
130(27)
540(12)
51
188
130(21)
319(28)
Tpan
321
117
Tbor
8
137
23
139
177
308
Tmag
140
403
Taes
9
49
97
81
176
127
Tbru
51
52
89
275
Tmela
153
119
Tind
λ = 0.036
λ = 0.163
B
M. sextelata (Msex)
T. panzihuhanense (Tpan)
C
Msex
NW_025408626.1
GH127
GH39
Tpan
ctg_7
Tpan
ctg_6
10 kb
10 kb
10 kb
Syntenic othologues
Non-syntenic orthologues
TE hotspot
private genes
D
Msex
NW_025408620.1
PL1_2
Tpan
ctg_2
10 kb
10 kb
E
Cumulative distribution
1.00
0.75
0.50
0.25
0.00
0
0.5
1
1.5
2
Length syntenic blocks (Mb)
Msex
Tpan
F
%TE coverage
100
75
50
25
0
**
Non syntenyc
Syntenyc
G
%Gene coverage
100
75
50
25
0
**
Non syntenyc
Syntenyc
H
Log(%TE coverage)
2.5
0.0
−2.5
**
**
**
**
**
**
All genes
Expanded Tpan
Expanded Tuberaceae
exons
Flanking (5 kb)
introns

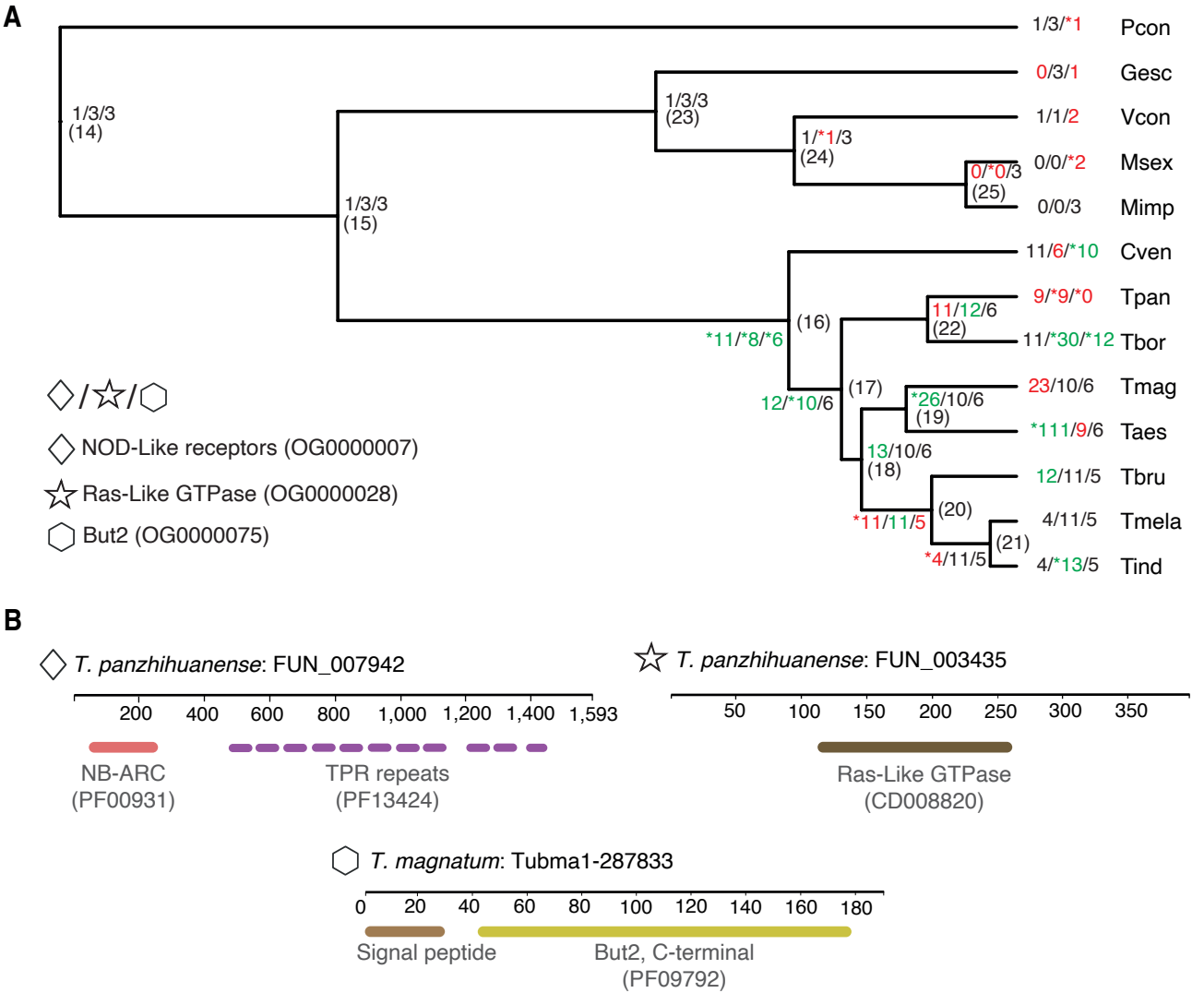
A
1/3/3
(14)
1/3/3
(15)
1/3/3
(23)
1/*1/3
(24)
0/*0/3
(25)
(16)
*11/*8/*6
11/12/6
(22)
(17)
12/*10/6
*26/10/6
(19)
13/10/6
(18)
(20)
*11/11/5
(21)
*4/11/5
1/3/*1 Pcon
0/3/1 Gesc
1/1/2 Vcon
0/0/*2 Msex
0/0/3 Mimp
11/6/*10 Cven
9/*9/*0 Tpan
11/*30/*12 Tbor
23/10/6 Tmag
*111/9/6 Taes
12/11/5 Tbru
4/11/5 Tmela
4/*13/5 Tind
NOD-Like receptors (OG0000007)
Ras-Like GTPase (OG0000028)
But2 (OG0000075)
B
T. panzhihuanense: FUN_007942
200 400 600 800 1,000 1,200 1,400 1,593
NB-ARC
(PF00931)
TPR repeats
(PF13424)
T. panzhihuanense: FUN_003435
50 100 150 200 250 300 350
Ras-Like GTPase
(CD008820)
T. magnatum: Tubma1-287833
0 20 40 60 80 100 120 140 160 180
Signal peptide
But2, C-terminal
(PF09792)

High-quality assembly of the Chinese white truffle genome and recalibrated divergence time estimate provide insight into the evolutionary dynamics of Tuberaceae

Jacopo Martelossi, Jacopo Vujovic, Yue Huang, et al.

Genome Res. published online August 21, 2025
Access the most recent version at doi:10.1101/gr.280368.124